ON THE FEASIBILITY OF MEASURING THE EARTH-ATMOSPHERE ENERGY BALANCE

by
Michael Adam Alexander

Scientific Report #7
September 1986

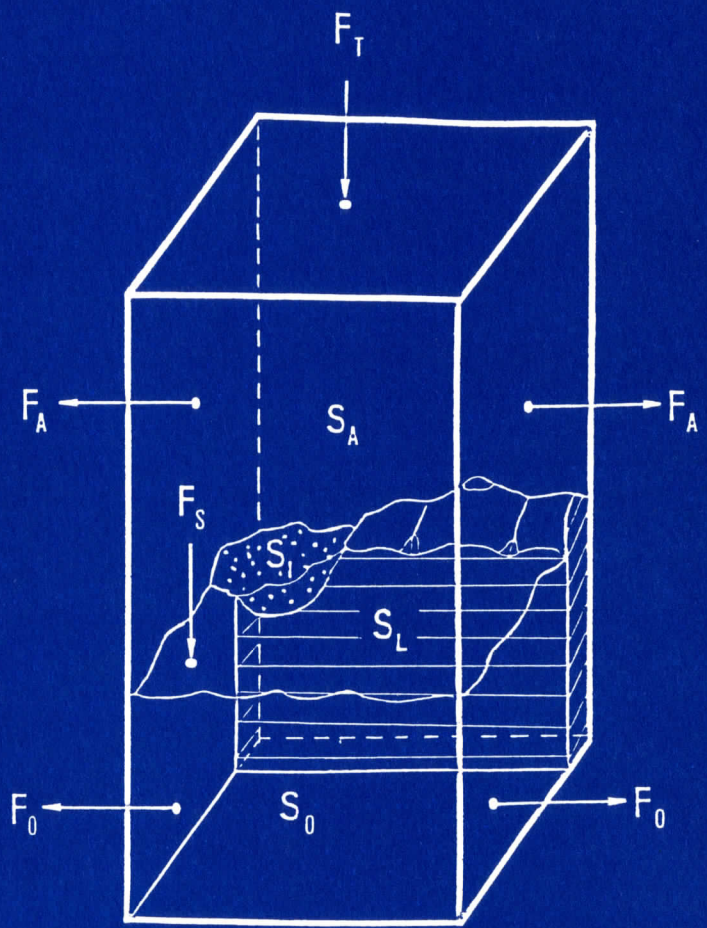

The research reported here has been supported by NASA Grant NSG-5223

Gerald F. Herman
Principal Investigator

Department of Meteorology
University of Wisconsin—Madison
1225 W. Dayton Street
Madison, Wisconsin 53706

Department of Meteorology
University of Wisconsin-Madison
Madison, Wisconsin 53706

ON THE FEASIBILITY OF MEASURING THE

EARTH-ATMOSPHERE ENERGY BALANCE

by

Michael Adam Alexander

Scientific Report #7

Support for this work was provided by the
National Aeronautics and Space Administration
under Grant NSG-5223.

Gerald F. Herman, Principal Investigator

Foreward

The substantial number of diagnostic studies that have been conducted with the data from the 1979 Global Weather Experiment have clearly illustrated that the use of the general circulation model as a data-handling tool is of comparable importance to its use in weather forecasting. The GCM-assimilated data sets have provided unique opportunities to conduct studies of the energetics and dynamics that would not have been possible based on conventional data alone.

Nonetheless, it would be a serious mistake to fail to recognize the consequences of using processed data sets to infer the behavior of the atmosphere. In many cases it may well be impossible to separate clearly the effects of the model from the true behavior of the atmosphere, however we may choose to define the latter.

This study which began initially with our investigation of the diabatic heating fields in the DST and FGGE data sets, focuses on the problems of inferring atmospheric flux divergences from assimilated data. The problem is of special importance given the current interest in "Cage"-type approaches to the problem of estimating the energy transport by the worlds oceans.

The work reported here constituted the MS thesis of Mr. Michael Alexander at the University of Wisconsin. The research was supported by NASA grant NSG-5223, and utilized the the FGGE data and computational resources provided by NASA's Goddard Laboratory for Atmospheres.

Gerald F. Herman

Associate Professor

10 September, 1986

Abstract

The earth-atmosphere energy balance is computed using the column budget technique described by Oort and Vonder Haar (1976). The results are used to assess the physical consistency and accuracy of energy balance calculations. Regional estimates of the atmospheric budget terms are obtained for the Special Observing Periods of the FGGE year utilizing observations assimilated by a four-dimensional analysis system. The terrestrial budget is dominated by the time rate of change and flux divergence of heat in the ocean. Ocean heat storage is obtained from ocean temperature observations with the heat flux divergence computed as a residual.

Both the atmosphere and ocean are shown to export a substantial amount of energy from the tropics to the midlatitudes. During winter the oceans supply large quantities of energy to the atmosphere which then transports the energy to the continental and polar heat sinks. The atmospheric exchange of energy between land and ocean is found to be much stronger in the Northern Hemisphere where continents are more extensive.

Sensitivity studies, error analyses, and comparison with other studies indicate that the error in the atmospheric energy flux divergence and the residually computed surface energy flux are on the order of 20 W m^{-2} and 30 W m^{-2}, respectively. Large uncertainties in the time tendency of ocean heat storage are estimated for periods of a season or less. We conclude that it is not yet possible to accurately estimate the ocean heat transport using the column budget technique.

TABLE OF CONTENTS

		Page
Foreward		ii
Abstract		iv
Table of Contents		v
List of Symbols		vii
I	Introduction	1
II	Basic theory	7
III	Model and Data	14
	A. Model and data assimilation system	14
	B. Atmospheric data	17
	C. Oceanic data	17
IV	Computations	20
	A. Regions	20
	B. Numerical methods	20
	C. Mass balance correction	24
V	Results and Discussion	26
	A. The atmospheric budget	26
	B. The oceanic budget	52
	C. Ocean heat transport	60
	D. Errors and sensitivities	64
	1. Data and data assimilation errors	65
	2. Model errors	66

3. Uncertainties in the budget method 67

a. Sensitivity to size and location of the budget box 68

b. Budget results in sigma vs. pressure coordinates 72

c. Residual vs. direct computation of the convective flux 77

d. Error propagation 77

VI Summary and Conclusion 86

Bibliography 92

Appendix I 99

Appendix II 103

Appendix III 106

Acknowledgements

List of Symbols

a	radius of the earth
A	Area
c_o	specific heat of ocean water
c_p	specific heat of air at constant pressure
d	depth in the ocean
div	horizontal divergence operator
E	total energy
F	Friction
F_A	horizontal transport of energy in the atmosphere
F_O	horizontal transport of energy in the ocean
F_S	vertical flux of energy at the surface
F_T	vertical flux of energy at the top of the atmosphere
g	gravity
K	kinetic energy, $1/2(V^2)$
M	the number of ocean sectors in a latitude belt
L	latent heat of evaporation
LH	latent heat flux at the surface
LW_S	flux of longwave radiation at the surface
LW_T	flux of longwave radiation at the top of the atmosphere
p	pressure
P_S	surface pressure
P_T	pressure at the top of the atmosphere
q	specific humidity of air

Q	vertically integrated diabatic heating rate in the atmosphere
R	net radiative flux at the surface
S	diabatic heating rate
S_A	rate of storage of energy in the atmosphere
S_I	rate of storage of energy in ice and snow
S_L	rate of storage of energy in land
S_O	rate of storage of energy in the ocean
SH	sensible heat flux at the surface
SW_A	shortwave radiation absorbed in the atmosphere
SW_S	shortwave radiation absorbed by the earth (ice, land, ocean)
t	time
T	temperature
$\vec{V}$	horizontal velocity vector
x	arbitrary scalar quantity
z	height
∇	horizontal divergence operator
ϕ	latitude
λ	longitude
ω	vertical velocity in pressure coordinates, dp/dt
ρ	density
σ	vertical coordinate, p/p_S
$\dot{\sigma}$	vertical velocity in sigma coordinates, $d\sigma/dt$

1. INTRODUCTION

The transport of energy by the atmosphere and ocean plays a significant role in determining the earth's climate. In addition, the ocean, and to a lesser extent the atmosphere, moderate the seasonal cycle by storing heat in summer and releasing it during winter. Energy budgets present a balanced account of the sources, sinks and the storage of energy, and the net flux of energy to or from a particular region. These methods have proven to be extremely useful in diagnosing mechanisms of energy generation, dissipation, and transfer in the atmosphere and ocean (eg. Sellers, 1965; Palmén and Newton, 1969). However, large gaps in the conventional data network (ie. radiosondes, ship reports, etc.), especially over the oceans, high latitudes, and Southern Hemisphere may greatly degrade budget analysis (Oort, 1978). General Circulation Models (GCMs) in conjunction with objective analysis schemes and data from several observing systems, have the potential to provide more accurate estimates of the energy budget components. The purpose of the present study is to assess the accuracy of regional energy balance calculations obtained from a combination of observations and model output.

With the advent of radiosondes in the 1940's, an aerological data network was established enabling atmospheric budget studies to be conducted. Studies which have examined the zonally averaged atmospheric energy balance include Gabites (1950), Newell et al. (1974), and Oort and Vonder Haar (1976). Due to the highly variable nature of some budget components, limited area energy statistics are

difficult to ascertain, though estimates have been made by Hastenrath (1966) for the Caribbean, Gruber (1970) for the Florida peninsula, and Alestalo (1981) for Europe.

Recent studies, such as Sävijarvi (1981), Lorenc and Swinbank (1984), Burridge (1985), and Holopainen and Fortelius (1986) have combined observations with GCM assimilation systems to obtain regional energy balance estimates. The assimilation procedure involves an extended GCM run with periodic data insertion to constrain the model to remain in a state close to that of the real atmosphere. Model-generated diagnostics obtained shortly after the data insertion are averaged to obtain mean energy balance statistics. The main benefit of using the model assimilation procedure is that it provides an automated and objective method of obtaining complete data sets. In addition, the model dynamics, conservation requirements and finite difference schemes which operate during the forecast period act to diminish inconsistencies in the data.

Studies using model-assimilated observations to investigate the atmospheric circulation and energy balance are prone to both random and systematic error (Lau and Oort, 1981; Lorenc and Swinbank, 1984). The incorporation of data into the model creates imbalances in the mass and energy fields. Alestalo (1981), Sävijarvi (1982) and others have shown that mass imbalances due to errors in the wind field can significantly affect energy balance calculations. A related problem is the spurious high frequency oscillations in the motion field caused by data insertion, which is only partially

removed by the model's finite differencing and smoothing schemes. Using multiple observing systems which have different sampling frequencies, densities and biases introduces added uncertainty into the budget analysis. Over areas where little data is available, the energy diagnostics are primarily obtained from model forecasts. In these areas, errors may arise due to inadequacies of the GCM's physics. These problems need to be addressed to determine the viability of using model assimilated data in diagnostic studies.

We examine regional atmospheric energy budgets using data from the First Global GARP Experiment (FGGE) data inserted into the Goddard Laboratory for the Atmospheres (GLA) 4-dimensional assimilation system. The model analysis is used to calculate the storage and flux divergence of the total energy in the atmosphere. The GCM's physical parameterizations supply the information necessary to calculate the radiative fluxes at the top of the atmosphere and the earth's surface. The flux of sensible and latent heat across the air-earth interface is derived as a residual from the atmospheric energy balance.

In contrast to calculations with atmospheric data, the direct computation of the energy budget components is extremely difficult in the ocean, due to the lack of water velocity measurements. Several techniques have been developed to indirectly estimate the ocean energy flux. Jung (1952) and Bryan (1962) showed that total energy in the ocean is accurately approximated by sensible heat alone. Five methods which have been used to calculate the ocean heat transport will be briefly discussed here: the dynamic, inverse,

surface budget, numerical, and column budget methods.

The dynamic method consists of computing surface currents from the curl of the wind stress, while deeper motions are assumed to be geostrophic and are calculated from the density field. The heat transport is then estimated from ocean temperature measurements and the computed velocity, e.g. Bryan (1962), Holland and Hirschman (1976), and Bryden and Hall (1980). Closely related to the dynamic method is the inverse technique, which has been employed by Wunsch (1978), Roemmich (1980), and Fu (1981). Mass conservation, geostrophic balance and additional constraints, such as the conservation of chemical tracers are applied in selected ocean regions. The heat transport through the regional boundaries is obtained by satisfying all the constraints to a desired level of accuracy.

The surface budget method balances the sources and sinks of energy at the air-sea interface with the heat stored within the ocean, the residual being equivalent to the vertically integrated heat flux divergence. The heat transport is computed by integrating the heat flux divergence over the boundary of the region. The surface budget method has been employed by Budyko (1963), Hastenrath (1982), and Hsuing (1985).

The numerical method utilizes a coupled atmosphere-ocean GCM to approximate the climatological mean state by prescribing the net radiation at the top of the atmosphere, and allowing the model to approach equilibrium. Using the output from coupled GCMs, Bryan (1969), Bryan et al. (1975) and Byran and Lewis (1979) have calculated the ocean heat transport. A variation on this approach is

to use a multi-year integration of an atmospheric GCM to generate estimates of the energy flux across the ocean surface. The surface energy budget method can then be used to compute the ocean heat transport (Pollard and Gates, 1982).

The present study uses the column budget method, which considers the energy in a vertical column extending from the top of the atmosphere to the ocean bottom. By computing the atmospheric energy balance we can obtain the net flux of energy from the atmosphere to the ocean. This energy is either stored as heat or removed via ocean currents. With ocean heat storage estimates from hydrographic temperature data, the ocean heat flux divergence is computed as a residual. The meridional heat transport is determined by selecting a boundary condition at the northern (southern) limit of an ocean basin and integrating the heat flux divergence in a southward (northward) direction. This method was used by Vonder Haar and Oort (1973), Oort and Vonder Haar (1976), and Carissimo et al. (1985).

Each of the five methods used to compute the oceanic heat transport is subject to numerous errors. Examining previous heat transport estimates obtained from these methods, Bretherton et al. (1982) found the estimates to vary by less than a factor of two, but believed the magnitude of the errors to be larger than this difference. The feasibility of using the column budget technique to determine the atmosphere-ocean energy balance depends on many factors which affect the accuracy of the budget calculations. Hastenrath (1980) indicated that error estimates, while essential to

budget studies, are unsatisfactory at present. The identification of the budget calculations most susceptible to error may suggest corrective measures which will improve energy balance estimates.

Five separate approaches are used here to investigate the accuracy of the energy balance components obtained from the column budget method:

1) Results from this and other studies are compared.

2) The sensitivity of computations to variations in the spatial domain is examined by changing the size and location of the regions.

3) Comparison of budget results is made using both pressure and sigma (normalized pressure) as the vertical coordinate in the atmosphere.

4) The combined surface sensible and latent heat flux obtained as a residual from the column budget method is contrasted to flux estimates from bulk aerodynamic formulae using surface wind, temperature, and moisture data.

5) Random and systematic errors in the atmospheric variables are prescribed and then inserted into the budget calculations to determine their impact on the estimates of the storage and flux divergence of energy.

II Basic Theory

The conservation of total energy in the earth-atmosphere system, can be expressed as (e.g. Oort and Vonder Haar, 1976)

$$\frac{\partial E}{\partial t} = F_T - \text{div } F_A - \text{div } F_O \qquad (1)$$

where E is the total energy, F_T is the net radiative flux at the top of the atmosphere and F_A and F_O are the vertically integrated fluxes of energy in the atmosphere and ocean, respectively. Eq. (1) states that the energy content of an atmosphere-ocean-land-ice column can change by the net radiation entering the top or by the divergence of energy transported by the atmosphere and ocean through the sides of the column. The transport of energy by ice and by atmospheric horizontal turbulent (i.e., subgrid scale) fluxes are neglected here, as are the direct effects of electrical, geothermal and biological processes.

The time rate of change of total energy

$$\frac{\partial E}{\partial t} = S_A + S_O + S_L + S_I, \qquad (2)$$

namely the sum of the time tendencies of energy stored in the atmosphere, S_A, ocean, S_O, land, S_L, and ice, S_I. In this study the energy stored by land and ice are assumed to be zero, the former because it is small compared to the oceanic storage (Gabites, 1950); the latter also appears to be small (Oort and Vonder Haar, 1976) but

is not well known. Defining downward fluxes to be positive, the net radiative flux at the top of the atmosphere,

$$F_T = SW_A + SW_S - LW_T \tag{3}$$

equals the shortwave radiation absorbed in the air column, SW_A, plus the shortwave radiation absorbed at the surface, SW_S, minus the outgoing longwave radiation at the top of the atmosphere, LW_T. P_S and P_T are, respectively, the pressure at the surface and the top of the atmosphere. This formulation is used to accommodate the GLA model diagnostics which computes the absorption of shortwave radiation and the flux of longwave radiation.

Combining the vertically integrated conservation equations for kinetic, thermal and latent energies (see Appendix I) the atmospheric storage and flux divergence terms are

$$S_A = \frac{\partial}{\partial t} \int_{P_T}^{P_S} (K + c_p T + Lq) \; dp/g \tag{4}$$

$$\text{div } F_A = \int_{P_T}^{P_S} (K + c_p T + gz + Lq)\vec{V} \; dp/g \tag{5}$$

where K is the kinetic energy, c_p the specific heat of air at constant pressure, T the temperature, L the latent heat of vaporization, q the specific humidity, gz the geopotential energy, $\vec{V}$ the horizontal wind vector, and g is gravity.

The time rate of change of storage and the flux divergence of energy in the ocean are, respectively,

$$S_O = \frac{\partial}{\partial t}\int_d^0 (K + c_o T + \frac{P}{\rho} + gz)\ \rho\ dz \qquad (6)$$

$$\text{div } F_O = \int_d^0 (K + c_o t + \frac{P}{\rho} + gz)\vec{V}\ \rho\ dz \qquad (7)$$

The pressure is denoted by P, the density by ρ, and c_o is the specific heat of liquid water. The vertical coordinate has been changed from pressure above the surface to height, z, below the surface. The depth, d, the lower boundary, is the level at which there are assumed to be no vertical fluxes of energy. With the assumption that the oceans are incompressible and hydrostatic, the pressure and height terms in the Eqs. (6) and (7) are of equal magnitude but opposite sign and therefore cancel each other. The kinetic energy in the ocean is neglected as it is several orders of magnitude smaller than the other terms. These approximations leave the sensible heat as the only remaining energy in S_O and F_O, as shown by Jung (1952) and with greater rigor by Bryan (1962).

The atmospheric budget is expressed as,

$$S_A = F_T - F_S - \text{div } F_A \qquad (8)$$

and the terrestrial (land-ocean-ice) budget by,

$$S_O = F_S - \text{div } F_O \qquad (9)$$

The net flux of energy at the surface F_S, includes the downward

radiative flux, R, (the absorbed shortwave flux minus the net upward longwave flux) minus the upward fluxes of sensible, SH, and latent heat, LH, written as

$$F_S = R - (SH + LH) \tag{10}$$

where the small amount of kinetic energy transferred from the atmosphere to the ocean is neglected.

By definition, the time and spatial average of quantity x are

$$\bar{x} = \frac{1}{t_2 - t_1} \int_{t_1}^{t_2} x \, dt$$

$$\langle x \rangle = \int_{\phi} \int_{\lambda} x a^2 \cos\phi \, d\lambda \, d\phi \Big/ \int_{\phi} \int_{\lambda} a^2 \cos\phi \, d\lambda \, d\phi$$

where t_2 and t_1 are the final and initial times, a the radius of the earth, λ the longitude, and ϕ the latitude. Then the time and area averages of equations (1), (8) and (9) are

$$\frac{\langle \partial \bar{E} \rangle}{\langle \partial t \rangle} = \langle \bar{F}_T \rangle - \langle \text{div } \bar{F}_A \rangle - \langle \text{div } \bar{F}_O \rangle \tag{11}$$

$$\langle \bar{S}_A \rangle = \langle \bar{F}_T \rangle - \langle \bar{F}_S \rangle - \langle \text{div } \bar{F}_A \rangle \tag{12}$$

$$\langle \bar{S}_O \rangle = \langle \bar{F}_S \rangle - \langle \text{div } \bar{F}_O \rangle \tag{13}$$

The energy budget of the earth atmosphere system is shown schematically in Fig. 1.

Substituting (10) into (12) and rearranging yields

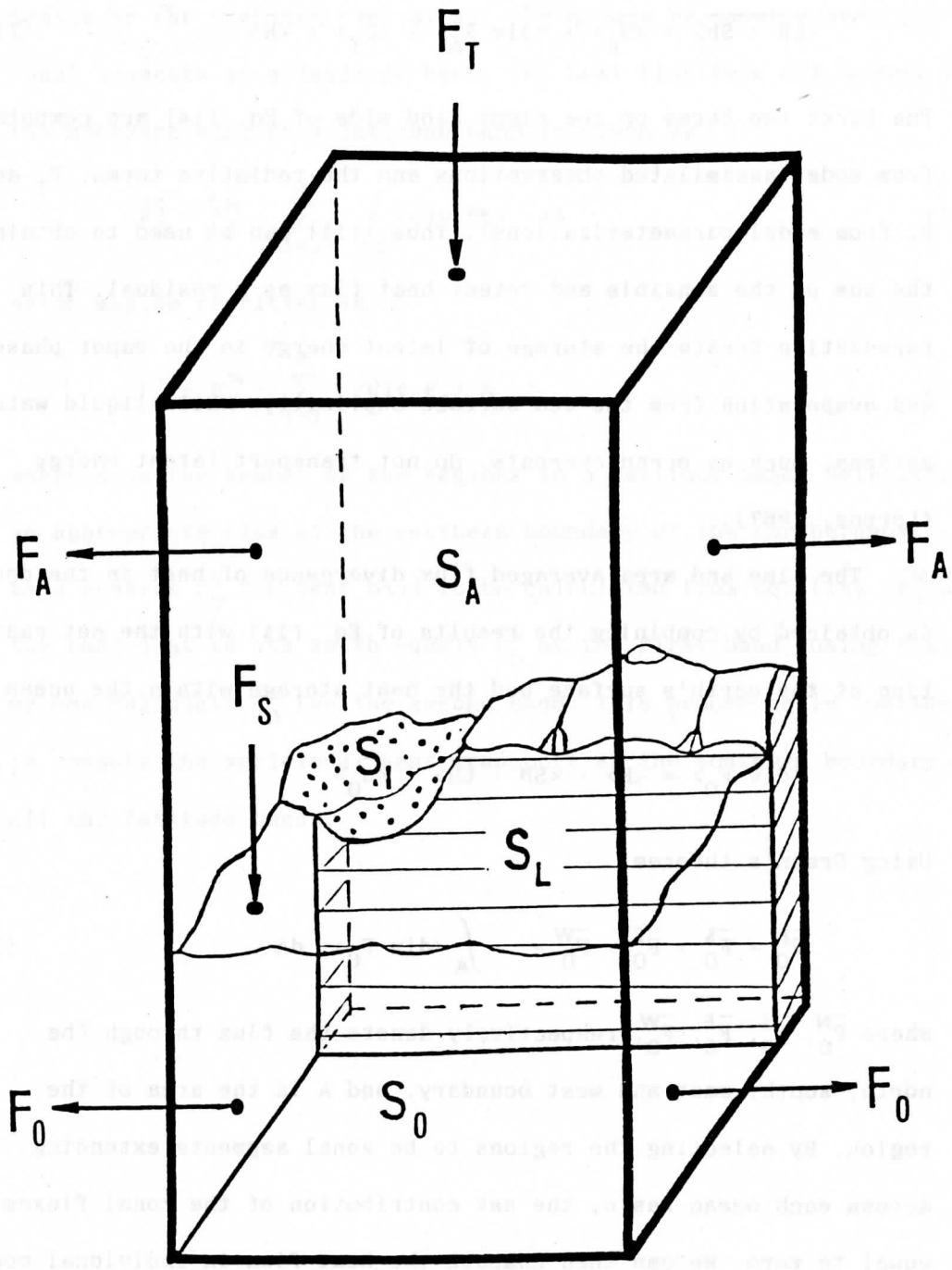

Fig. 1. Schematic of the earth-atmosphere energy balance. Adapted from Oort and Vonder Haar (1976).

$$\overline{\langle LH + SH \rangle} = \langle \bar{S}_A \rangle + \langle \text{div } \bar{F}_A \rangle - \langle \bar{F}_T \rangle + \langle \bar{R} \rangle \qquad (14)$$

The first two terms on the right hand side of Eq. (14) are computed from model assimilated observations and the radiative terms, F_T and R, from model parameterizations*. Thus, (14) can be used to obtain the sum of the sensible and latent heat flux as a residual. This formulation treats the storage of latent energy in the vapor phase and evaporation from the sea surface explicitly, while liquid water motions, such as ocean currents, do not transport latent energy (Lorenz, 1967).

The time and area averaged flux divergence of heat in the ocean is obtained by combining the results of Eq. (14) with the net radiation at the earth's surface and the heat storage within the ocean

$$\langle \text{div } \bar{F}_O \rangle = \langle \bar{R} \rangle - \overline{\langle SH + LH \rangle} - \langle \bar{S}_O \rangle \qquad (15)$$

Using Green's theorem,

$$\bar{F}_O^N - \bar{F}_O^S + \bar{F}_O^E - \bar{F}_O^W = \int_A \langle \text{div } F_O \rangle \, dA \qquad (16)$$

where $\bar{F}_O^N$, $\bar{F}_O^S$, $\bar{F}_O^E$, $\bar{F}_O^W$, respectively denote the flux through the north, south, east and west boundary, and A is the area of the region. By selecting the regions to be zonal segments extending across each ocean basin, the net contribution of the zonal fluxes is equal to zero. We can then compute the heat flux in individual ocean

---

* Most atmospheric budget studies (eg. Oort and Vonder Haar) use satellite observations to obtain the net radiation at the top of the atmosphere. The GLA GCM's radiation parameterizations are fairly comprehensive, though we plan to inter-compare model and satellite estimates of F_T to substantiate the accuracy of the model results.

basins or the combined flux of all the oceans by summing over the zonal segments in a latitude band. The heat flux from all oceans at the southern edge of a latitude band is given by

$$\bar{F}_0^S = \bar{F}_0^N - \sum_{i=1}^{M} \int_A \langle \text{div } F_0 \rangle \, dA \tag{17}$$

which may be rewritten as

$$\bar{F}_0^S = \bar{F}_0^N - \sum_{i=1}^{M} \langle \text{div } F_0 \rangle \, A \tag{18}$$

where M is the number of the regions in a latitude band. Selecting an appropriate flux at the northern boundary of the northernmost band enables $\bar{F}_0^S$ for that band to be calculated from Eq. (18). $\bar{F}_0^N$ of the band just to its south equals $\bar{F}_0^S$ of the first band; using (18) we can calculate $\bar{F}_0^S$ for the second band. This procedure is continued to compute the meridional heat transport at the southern boundary of all the latitude bands.

III Model and Data

A. The model and data assimilation system

The GLA GCM (see Kalnay et al. 1983) is a 9-layer, sigma coordinate, primitive equation model with a horizontal resolution of 4^{o} latitude by 5^{o} longitude. The model utilizes a fourth order differencing scheme on an unstaggered grid which conserves energy, and, in combination with a sixteen point Shapiro (1970) filter, approximately conserves enstrophy and mass. The cloud, radiation and surface flux parameterizations used in the model are described in Appendix II.

The GCM is part of a 4-dimensional analysis system used to process observations into global fields. These fields are the basis for our calculations of storage and flux divergence of energy in the atmosphere. In addition, the model's parameterizations provide the radiation terms in the budget equations and estimates of the surface sensible and latent heat flux. The sum of the model generated surface flux estimates will be compared to the residually derived values given by Eq. (14), the atmospheric energy balance equation.

The atmospheric diagnostics are extracted from a cyclic assimilation procedure (see Fig. 2), where data are periodically inserted into an extended model integration. The method of data insertion developed at GLA (Baker, 1983) interpolates the data to fixed coordinates in both time and space. A preprocessor corrects or deletes gross errors and orders the data by latitude and longitude. The data are assimilated every 6 hours by grouping the observations

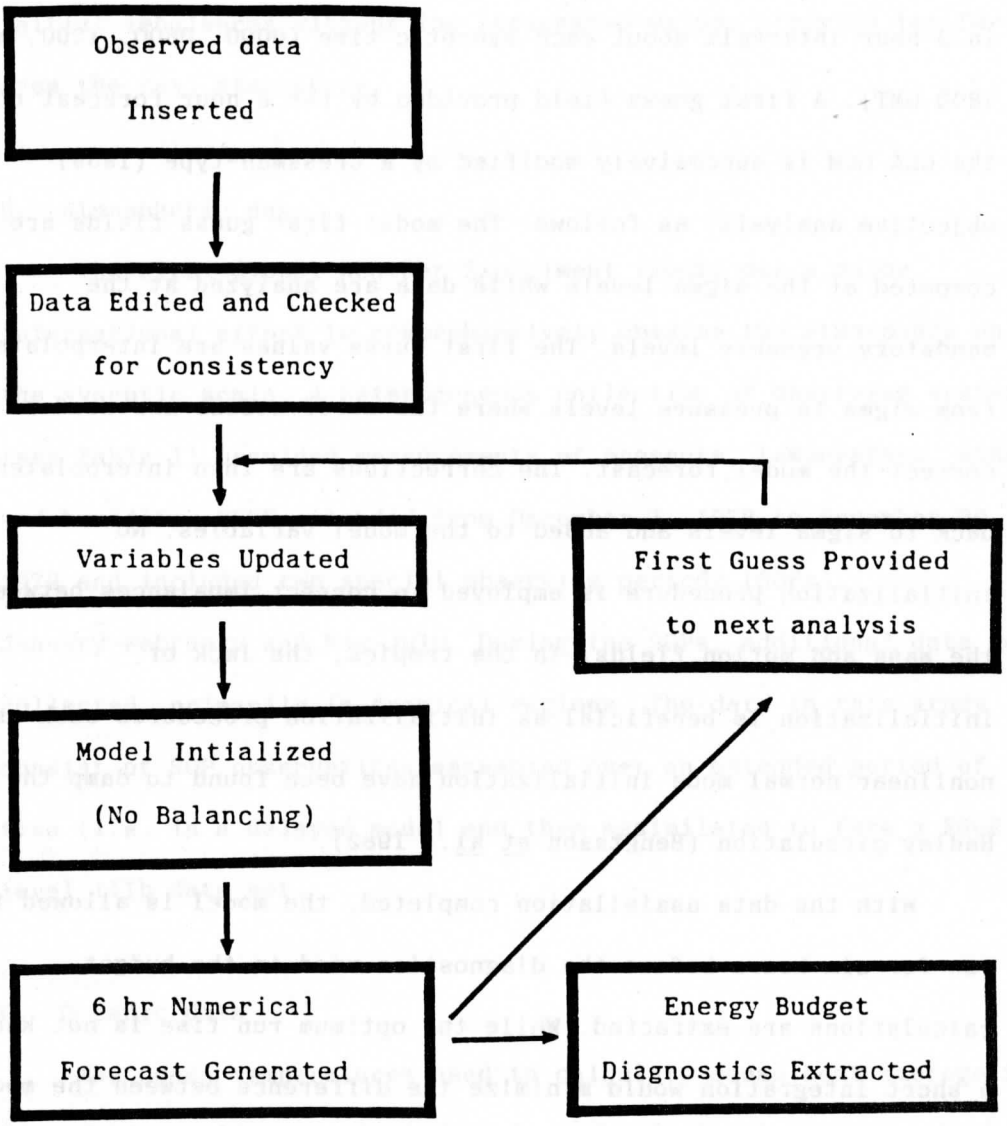

Fig. 2. Schematic diagram of the assimilation procedure and method of obtaining the energy budget diagnostics. Adapted from Baker (1982).

in 3-hour intervals about each synoptic time (0000, 0600, 1200, and 1800 GMT). A first guess field provided by the 6 hour forecast of the GLA GCM is succesively modified by a Cressman-type (1959) objective analysis, as follows. The model first guess fields are computed at the sigma levels while data are analyzed at the mandatory pressure levels. The first guess values are interpolated from sigma to pressure levels where the observations are used to correct the model forecast. The corrections are then interpolated back to sigma levels and added to the model variables. No initialization procedure is employed to correct imbalances between the mass and motion fields. In the tropics, the lack of initialization is beneficial as initialization procedures such as nonlinear normal mode initialization have been found to damp the Hadley circulation (Bengtsson et al., 1982).

With the data assimilation completed, the model is allowed to run for six hours before the diagnostics used in the budget calculations are extracted. While the optimum run time is not known, a short integration would minimize the difference between the model forecast and the true atmosphere. A longer run allows the model dynamics, time differencing and spatial smoothing schemes to suppress spurious oscillations caused by data insertion. In addition, a longer integration enables the model parameterizations of diabatic processes to adjust to the new initial conditions. Schubert and Herman (1981) indicated that this adjustment may take an extended period of time, perhaps longer than a week. Sampling the model run six hours after data insertion is an attempt to constrain the

initial imbalances without the forecasted values straying too far from the real atmosphere.

B. Atmospheric data

The First Global Weather Experiment (FGGE) was a major international effort to comprehensively observe the atmosphere on the synoptic scale. A heterogeneous collection of observing systems (see Table 1) provided measurements of pressure, temperature, wind and humidity. FGGE extended from December 1, 1978 to November 30, 1979 and included two special observing periods (SOPs), January-February and May-July. During the SOPs, additional data were collected, primarily in tropical regions. The data in this study consist of SOP observations assembled over an extended period of time (i.e. in a delayed mode) and then assimilated to form a FGGE level IIIb data set.

C. Oceanic data

The ocean temperatures used to calculate ocean heat storage, S_0, are based on climatological data from the National Oceanographic Data Center (NODC) compiled by Levitus (1982). Due to a lack of synoptic oceanographic data for individual years, monthly mean temperature fields based on all observations regardless of the year are used to compute S_0. The data set consists of approximately 500,000 casts from hydrographic stations collected through the first quarter of 1977 and about 785,000 from bathythermographs collected as of the first quarter of 1978. The observations were interpolated

TABLE 1. Data used from FGGE observing systems. TWOS denote tropical wind observing ship, AIDS aircraft integrated data system, ASDAR aircraft to satellite data relay, CTW cloud-track winds, and NESS National Environmental Satellite Service. Adapted from Baker (1983).

	Variable analyzed				
Observing system	pressure	height	temperature	wind	humidity
Rawinsondes		X		X	X
Pilot balloons				X	
TWOS NAVAIDS		X		X	X
Dropwindsondes		X		X	X
Tiros-N		X			
VTPR		X			
Aircraft			X	X	
AIDS			X	X	
ASDAR				X	
NESS CTW				X	
European CTW				X	
Wisconsin CTW				X	
Constant level balloons				X	
Surface Stations	X		X		
Ships	X		X	X	
Drifting buoys	X		X		
Environmental bouys	X		X		

to 19 NODC standard constant depth levels located between the surface and 1000 m. For a given month, all available data in a given month in 1^{o}x 1^{o} ocean squares are checked for errors and then averaged at each of the 19 levels. An objective analysis consisting of a Cressman-type (1959) scheme and five point smoother provides temperature values at grid points with no data and reduces the effects of spurious values.

IV Computations

A. Regions

Regions 1-5 (Fig. 3) were selected to compare the results obtained here to those of other studies. Zonal segments with latitudinal widths of 32^{o}, regions 11-19 (Fig.4), and 20^{o}, regions 20^{o}-34^{o} (Fig. 5), were employed to compute the meridional heat flux in the oceans. Narrower bands were not chosen as it was felt the results would be significantly affected by noise. In addition, regions 1-19 cover a majority of the globe between 70^{o}N and 70^{o}S and are used to investigate climatic differences between various areas of the earth. Regions 35-39 (Section 5D, Fig. 6) are utilized to investigate the sensitivity of the calculations to size and location of the budget box.

B. Numerical methods

Time derivatives of atmospheric variables are represented by first order finite difference approximations. Little difference was found between the second and fourth order approximations of the atmospheric flux divergence of energy, and only the results from the second order representation are given. Second order formulations are used to represent the time rate of change of heat in the ocean, as the data are given as monthly averages. Vertical integrals are computed by fitting a cubic spline to the data and then integrating the resulting polynomial. In the atmosphere, integrations are performed between 50 mb and the area averaged surface pressure,

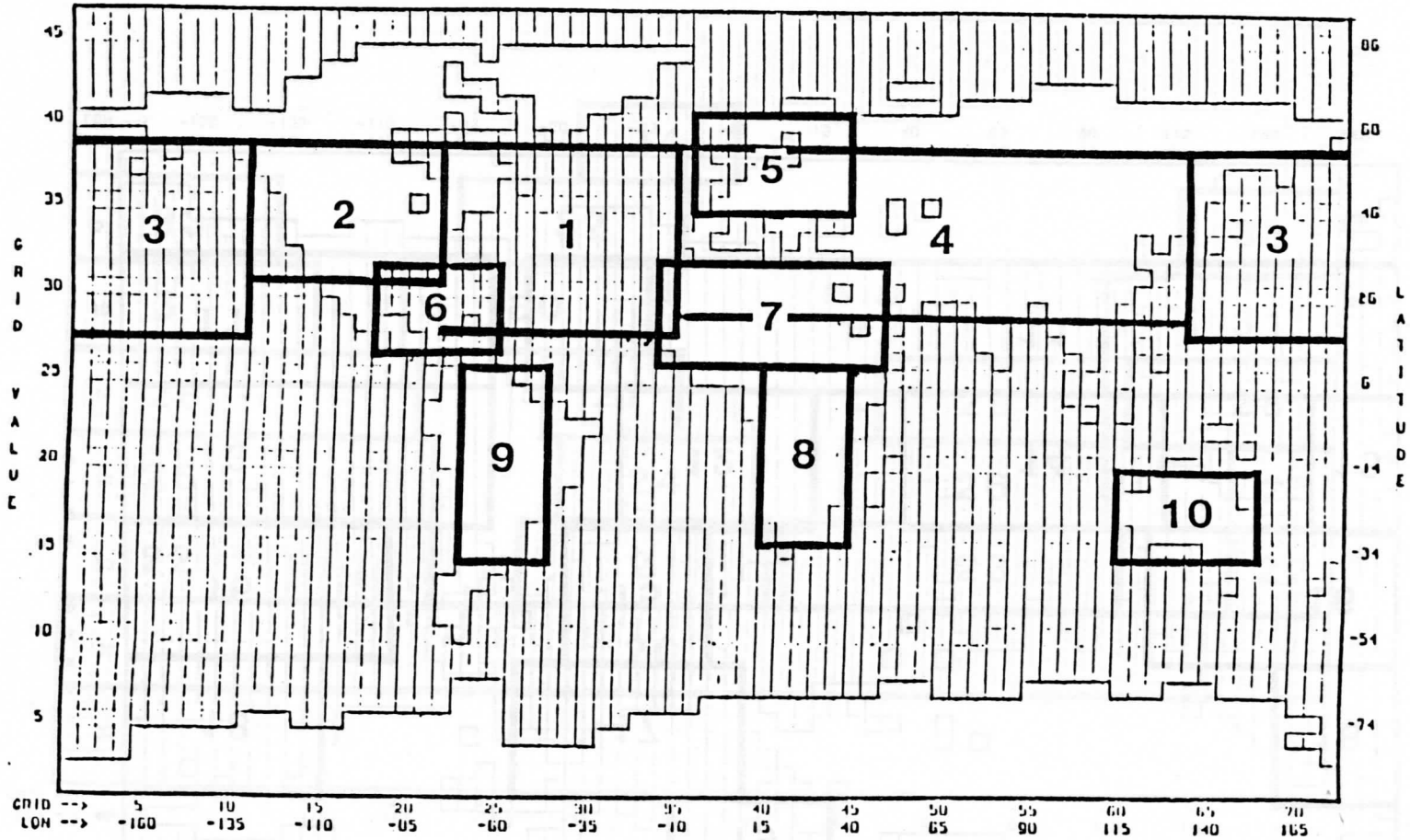

Fig. 3. Regions 1 through 10.

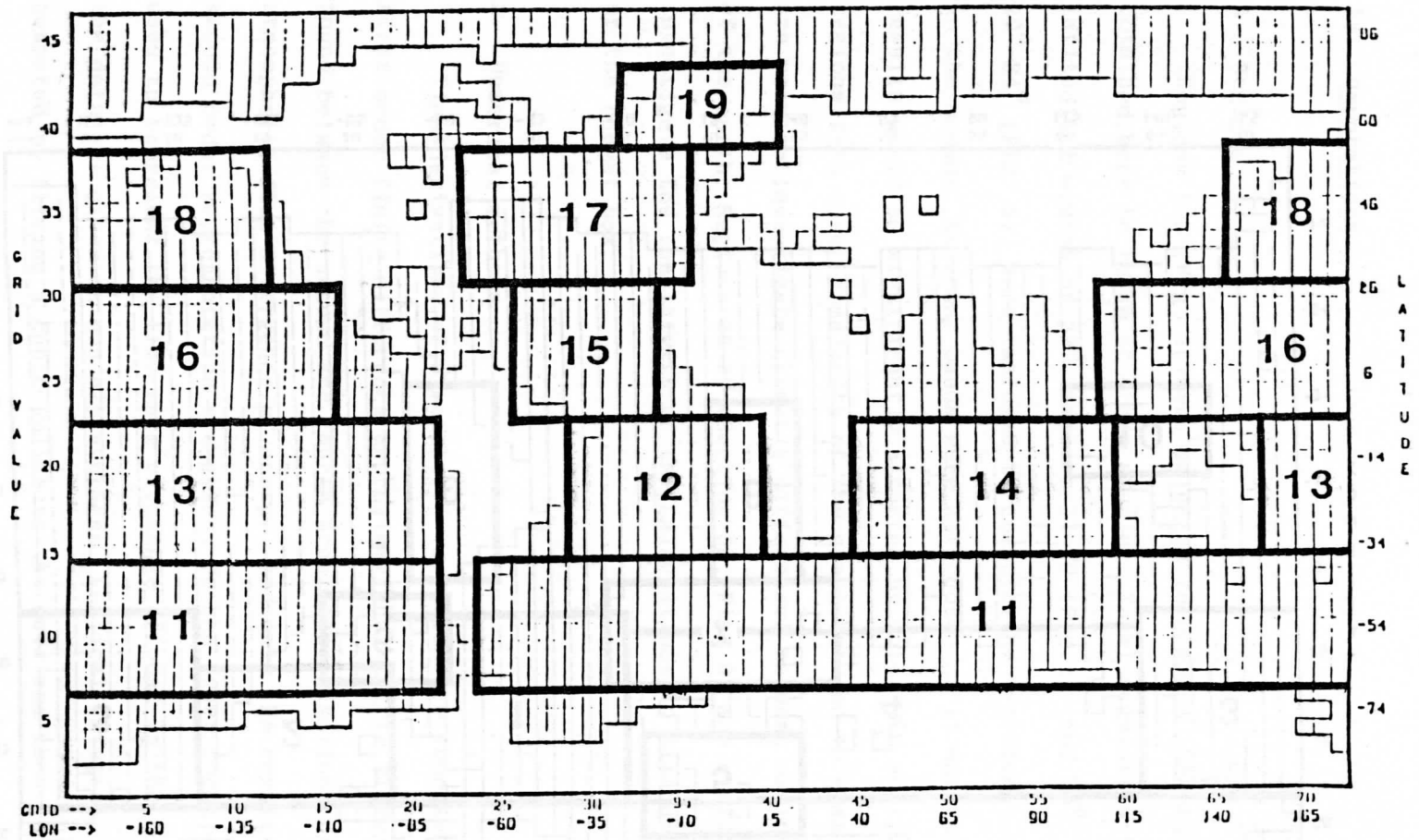

Fig. 4. Regions 11 through 19; 32^{o} ocean segments.

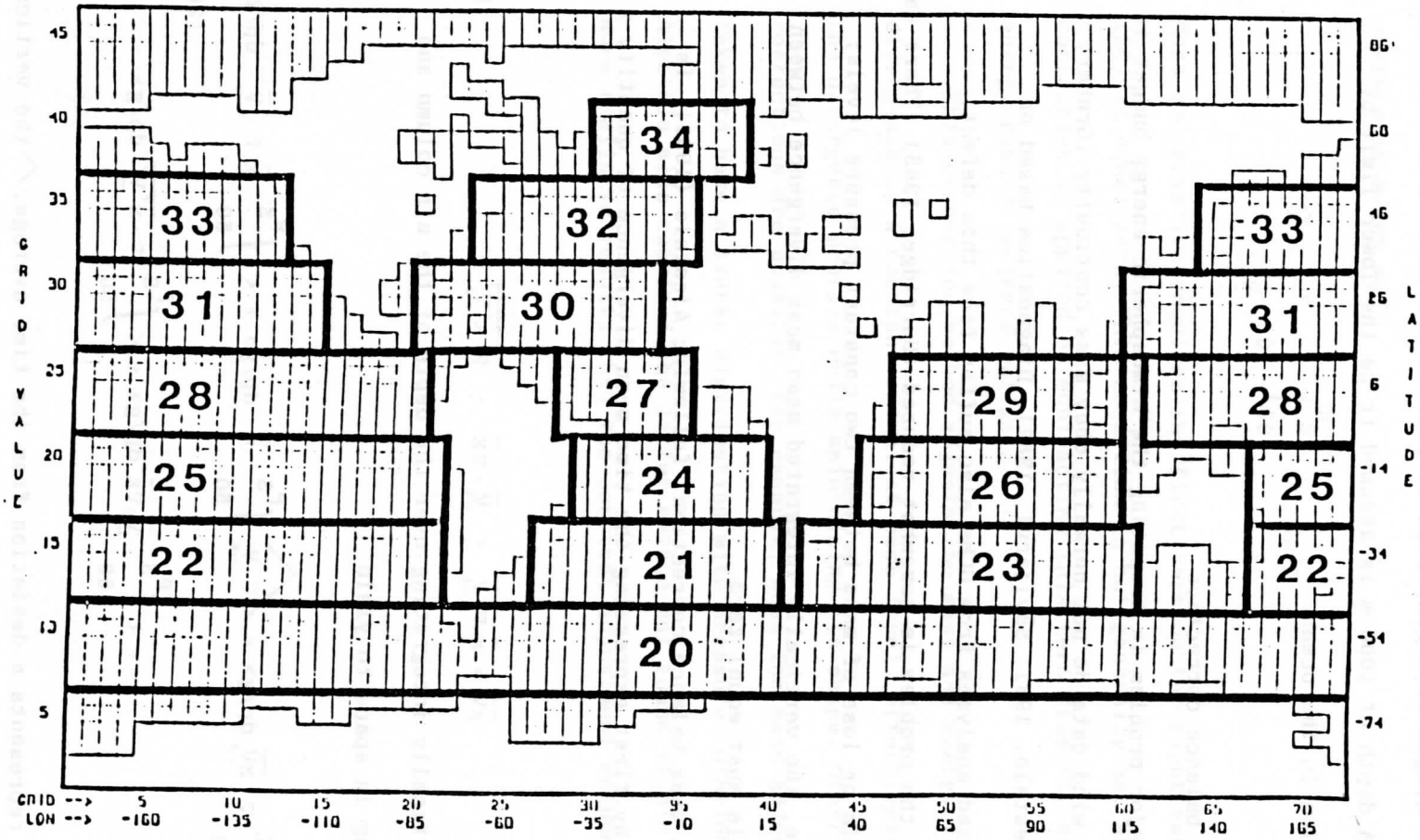

Fig. 5. Regions 20 through 34; 20^{o} ocean segments.

where the diagnostics generated at 1000 mb are used as the surface values. A depth of 1000 m is assumed to be the lower limit of integration in the ocean.

C. Mass balance correction

A major problem in computing the atmospheric energy budget is that the wind data do not normally obey mass continuity (Gruber, 1970; Alestalo, 1981; Sävijarvi, 1982). Diagnostics based on initialized analyses from GCMs also suffer from this defect, although the problem is somewhat reduced (Burridge, 1985). There can be no gain or loss of mass between two constant pressure levels; therefore, the vertically integrated mean mass divergence between the levels must equal zero.

The mass balance correction, following Alestalo (1981), is derived by first expressing the time mean divergence of quantity x as

$$\overline{x\mathbf{V}} = \bar{x}\,\nabla\cdot\bar{\mathbf{V}} + \bar{\mathbf{V}}\cdot\nabla\bar{x} + \nabla\cdot\overline{x'\mathbf{V}'} \tag{19}$$

then vertically integrating over the depth of the air column and averaging in space to yield

$$\left\langle \int_{50}^{P_S} \nabla\cdot\overline{x\mathbf{V}}\, dp/g \right\rangle = \left\langle \widehat{\nabla\cdot\bar{\mathbf{V}}} \int_{50}^{P_S} \bar{x}\, dp/g \right\rangle + \left\langle \int_{50}^{P_S} \bar{x}\,\nabla\cdot\bar{\mathbf{V}}^{+}\, dp/g \right\rangle + \left\langle \int_{50}^{P_S} \bar{\mathbf{V}}\cdot\nabla\bar{x}\, dp/g \right\rangle + \left\langle \int_{50}^{P_S} \nabla\cdot\overline{x'\mathbf{V}'}\, dp/g \right\rangle \tag{20}$$

where $'$ represents a deviation from the time average, $\widehat{\ }$ the vertical

average and + a deviation from the vertical average. The vertical average is given as

$$\hat{x} = \frac{g}{P_S - 50} \int_{50}^{P_S} x \; dp/g$$

Mass conservation requires the first term on the right hand side of (20) to equal zero. This condition is not generally met and a correction is applied by subtracting this term from the original energy flux divergence estimate.

This correction method adjusts the mass and energy flux divergence by a constant amount at each level, effectively shifting the divergence profile while maintaining its shape. Other corrections are possible, for example, when the mass adjustment is taken to have a linear distribution with pressure (O'Brien, 1970). Alestalo also examined the latter method but found it did not yield more realistic results than the constant adjustment method.

V Results and Discussion

A. The atmospheric budget

The net radiative flux at the top of an atmospheric column, F_T, is balanced by changes in the storage of energy within the column, S_A, the divergence of the energy transport between the column and the surrounding air, div F_A, and the flux of energy between the air and ground, F_S, as given by Eq. (12). The results presented for these energy balance components are obtained from five months of data during 1979 and differ from the long-term climatic average. The extensive data set acquired during the FGGE year provides an excellent base to examine techniques for estimating the earth-atmosphere energy balance.

The energy budgets are computed for each month of the Special Observing Periods (SOPs) and for the duration of both periods. The first period includes January and February while May, June and July comprise the second period. The results presented for January include data from 5 January to 5 February and likewise the February results extend from 5 February to 5 March. Three tables are presented for each of the atmospheric components, a table for the "climatic regions" (regions 1-10), the 32^o zonal segments (regions 11-19), and for the 20^o zonal segments (regions 20-34). The results from this study will be compared to those of Oort and Vonder Haar (1976).

The net radiation at the top of the atmosphere, F_T, is presented in Tables 2-4 for regions 1-34. The results show that

TABLE 2. Net incoming radiation at the top of the atmosphere (W m^{-2})

Region	Latitude	Longitude	Location	Jan	Feb	Jan-Feb	May	June	July	May-July
1	20N-60N	72.5W- 12.5W	N. Atlantic	-23	31	3	182	201	187	191
2	28N-60N	122.5W- 72.5W	N. America	-36	10	-15	158	184	157	164
3	20N-60N	137.5E-122.5W	N. Pacific	-23	29	1	183	204	177	186
4	24N-60N	12.5W-137.5E	Eurasia	-11	30	9	172	171	148	166
5	44N-68N	7.5W- 37.5E	Europe	-98	-52	-76	126	142	130	135
6	12N-32N	97.5W- 62.5W	Caribbean	33	79	54	148	138	128	137
7	8N-32N	17.5W- 47.5E	N. Africa	74	118	96	154	145	140	148
8	32S- 8N	12.5E- 37.5E	S. Africa	117	128	124	82	67	62	72
9	36S- 8N	72.5W- 47.5W	S. America	124	122	123	68	61	66	65
10	36S-16S	112.5E-152.5E	Australia	177	154	167	43	25	43	38

TABLE 3. Net incoming radiation at the top of the atmosphere (W m^{-2})

Region	Latitude	Longitude	Location	Jan	Feb	Jan-Feb	May	June	July	May-July
11	68S-36S	67.5W- 77.5W	Antarctic O.	195	137	168	-81	-103	-91	-92
12	36S- 4S	42.5W- 12.5E	Atlantic O.	187	175	183	74	47	55	60
13	36S- 4S	152.5E- 77.5W	Pacific O.	169	170	168	67	43	50	52
14	36S- 4S	37.5E-112.5E	Indian O.	162	150	158	54	26	33	39
15	4S-28N	57.5W- 17.5W	Atlantic O.	65	108	86	157	151	155	155
16	4S-28N	107.5E-107.5W	Pacific O.	55	98	74	143	143	145	142
17	28N-60N	72.5W- 7.5W	Atlantic O.	-58	-4	-32	180	205	186	191
18	28N-60N	142.5E-127.5W	Pacific O.	-54	-5	-32	182	216	183	191
19	60N-80N	27.5W- 17.5E	Atlantic O.	-126	-111	-119	108	131	110	118

TABLE 4. Net incoming radiation at the top of the atmosphere (W m^{-2})

Region	Latitude	Longitude	Location	Jan	Feb	Jan-Feb	May	June	July	May-July
20	68S-48S	Continous band	Antarctic O.	179	105	144	-111	-128	-116	-118
21	48S-28S	52.5W- 17.5E	Atlantic O.	217	174	198	-20	-49	-29	-32
22	48S-28S	147.5E- 77.5W	Pacific O.	214	178	195	-22	-43	-44	-37
23	48S-28S	22.5E-117.5E	Indian O.	213	183	200	-13	-48	-34	-31
24	28S- 8S	42.5W- 12.5E	Atlantic O.	184	170	179	86	56	64	70
25	28S- 8S	147.5E- 77.5W	Pacifc O.	160	166	160	79	51	62	62
26	28S- 8S	37.5E-112.5E	Indian O.	153	138	148	60	32	40	45
27	8S-12N	47.5W- 7.5W	Atlantic O.	82	112	97	102	94	109	103
28	8S-12N	117.5E- 82.5W	Pacific O.	82	105	92	109	103	116	108
29	8S-12N	47.5E-112.5E	Indian O.	86	121	104	115	103	104	109
30	12N-32N	87.5W- 17.5W	Atlantic O.	43	97	69	189	188	181	187
31	12N-32N	112.5E-112.5W	Pacific O.	33	92	60	187	192	180	185
32	32N-52N	72.5W- 7.5W	Atlantic O.	-58	-2	-31	181	209	189	194
33	32N-52N	132.5E-122.5W	Pacific O.	-48	0	-26	186	220	183	195
34	52N-72N	37.5W- 7.5E	Atlantic O.	-114	-88	-101	147	173	159	161

tropical and subtropical regions, those located between 32°N and 36°S, receive a surplus of energy for all months, with larger values found in the summer hemisphere. The mid- and high-latitude regions reflect the annual cycle with energy loss during winter and energy gain during summer. Maximum values of F_T exceeding 200 W m^{-2} are found in the midlatitudes of both hemispheres during summer. With the exception of Eurasia during winter, the Northern Hemisphere continents receive less energy via F_T then the oceanic regions during both winter and summer, a result which has also been documented by Bretherton et al. (1982). This phenomenon is attributed in part to the higher albedo of land which causes more solar radiation to be reflected to space.

The values obtained for F_T tend to exceed the zonal averages given by Oort and Vonder Haar (1976) and the global values of Stephens et al. (1981) by an estimated 20-40 W m^{-2}. The largest differences seem to occur over the oceans in the summer hemisphere. From Eq. (3) we see that the net radiation is composed of three terms, the shortwave radiation absorbed in the atmosphere, SW_A, the shortwave radiation absorbed at the surface, SW_S, and the longwave radiative flux at the top of the atmosphere, LW_T. The LW_T values are visually compared to the satellite estimates of Janowaick et al. (1985) and are qualitatively similar. Our SW_A values are smaller than those derived from the radiative transfer calculations given by Freeman and Liou (1979), while our estimates of shortwave radiation absorbed at the ocean surface are generally larger then those of Esbensen and Kushnir (1981). The discrepacies in the F_T estimates

are probably caused by the GLA model overestimating SW_S. Mintz (personal communication) attributes this bias to the GLA GCM parameterization of shortwave radiation absorption by cumulus clouds.

Other atmospheric models, such as the NCAR Climate Model and Oregon State GCM, produce SW_S values which are systematically higher than observed values (Kutzbach, personal communication; Pollard and Gates, 1982). Using satellite observations coupled with a radiative transfer model Stephens et al. (1981) found the values of shortwave energy absorbed at the earth's surface to be larger than those of London (1957); for tropical oceans this difference was calculated to be 35 W m^{-2}.

The time rate of change of energy stored in the atmosphere, S_A, is given in Tables 5-7. The energy is stored in three forms, kinetic, sensible (which is composed of internal energy plus pressure work effects), and latent energy. The majority of the storage changes are due to fluctuations in atmospheric sensible and latent heat. The time tendency of kinetic energy for all regions is generally less than 1 W m^{-2} and is often neglected in energy budget studies. Oort and Vonder Haar (1976) found the values of S_A to be small for all 12 months in the tropics and for all latitude bands in the Northern Hemisphere during January and February. Their results also indicate a steady increase in the rate of atmospheric energy storage north of 20^{o}N from February to May which then declines and approaches zero by July. We found large values of S_A in the tropics and at all latitudes for the months of January, February and July.

TABLE 5. Time rate of change of energy stored in the atmosphere (W m^{-2})

Region	Latitude	Longitude	Location	Jan	Feb	Jan-Feb	May	June	July	May-July
1	20N-60N	72.5W- 12.5W	N. Atlantic	7	-6	1	6	7	12	10
2	28N-68N	122.5W- 72.5W	N. America	11	16	13	22	14	13	17
3	20N-60N	137.5E-122.5W	N. Pacific	0	3	2	15	10	9	12
4	24N-60N	12.5W-137.5E	Eurasia	2	1	2	18	18	8	15
5	44N-68N	7.5W- 37.5E	Europe	18	13	16	35	-1	10	12
6	12N-32N	97.5W- 62.5W	Caribbean	15	-10	3	9	7	-6	4
7	8N-32N	17.5W- 47.5E	N. Africa	1	3	2	13	5	7	8
8	32S- 8N	12.5E- 37.5E	S. Africa	2	-1	0	-8	-11	-4	-7
9	36S- 8N	72.5W- 47.5W	S. America	0	1	0	-6	7	2	1
10	36S-16S	112.5E-152.5E	Australia	-3	13	5	-19	-1	-4	-8

TABLE 6. Time rate of change of energy stored in the atmosphere (W m^{-2})

Region	Latitude	Longitude	Location	Jan	Feb	Jan-Feb	May	June	July	May-July
11	68S-36S	67.5W- 77.5W	Antarctic O.	2	2	2	-5	-13	4	-4
12	36S- 4S	42.5W- 12.5E	Atlantic O.	-5	-3	-4	-2	-9	-4	-5
13	36S- 4S	152.5E- 77.5W	Pacific O.	1	-2	0	-7	-2	-7	-5
14	36S- 4S	37.5E-112.5E	Indian O.	4	0	2	-17	0	-4	-8
15	4S-28N	57.5W- 17.5W	Atlantic O.	-4	3	-1	6	-5	3	2
16	4S-28N	107.5E-107.5W	Pacific O.	-7	1	-3	-3	6	0	1
17	28N-60N	72.5W- 7.5W	Atlantic O.	11	-8	2	8	11	15	12
18	28N-60N	142.5E-127.5W	Pacific O.	5	0	3	19	9	12	13
19	60N-80N	27.5W- 17.5E	Atlantic O.	-7	6	-1	23	2	14	15

TABLE 7. Time rate of change of energy stored in the atmosphere ($W\ m^{-2}$)

Region	Latitude	Longitude	Location	Jan	Feb	Jan-Feb	May	June	July	May-July
20	68S-48S	Continous band	Antarctic O.	3	2	3	-5	-13	4	-5
21	48S-28S	52.5W- 17.5E	Atlantic O	3	-7	-2	-6	-23	15	-3
22	48S-28S	147.5E- 77.5W	Pacific O.	4	-5	0	-5	-7	-4	-5
23	48S-28S	22.5E-117.5E	Indian O.	-6	12	3	-8	-4	-4	-6
24	28S- 8S	42.5W- 12.5E	Atlantic O.	-4	-2	-3	-4	-5	-5	-5
25	28S- 8S	147.5E- 77.5W	Pacific O.	-1	-1	-1	-9	-1	-9	-6
26	28S- 8S	37.5E-112.5E	Indian O.	5	-2	2	-20	3	-1	-8
27	8S-12N	47.5W- 7.5W	Atlantic O.	0	7	3	14	-13	-3	-1
28	8S-12N	117.5E- 82.5W	Pacific O.	0	-6	-3	-8	3	-2	-3
29	8S-12N	47.5E-112.5E	Indian O.	10	-9	1	4	-11	0	-3
30	12N-32N	87.5W- 17.5W	Atlantic O.	5	-7	-1	2	5	3	4
31	12N-32N	112.5E-112.5W	Pacific O.	-10	5	-2	3	11	4	6
32	32N-52N	72.5W- 7.5W	Atlantic O.	9	-1	4	9	13	14	14
33	32N-52N	132.5E-122.5W	Pacific O.	7	-2	3	20	14	14	15
34	52N-72N	37.5E- 7.5E	Atlantic O.	-3	-7	-5	23	-1	23	16

In addition, large month to month fluctuations in S_A are seen in all regions.

The difference between the two studies' estimates of S_A may be due in part to the method of calculation. Oort and Vonder Haar (1976) averaged five years of monthly mean energy values and computed the difference between the following and preceeding month to obtain S_A. In the present study, S_A is calculated by taking the difference in energy between the final and initial time period and reflects the current rather than the climatological state of the atmosphere. When S_A is recomputed for June by subtracting the average May from the average July value, the results are similar to the the zonally averaged values given by Oort and Vonder Haar, as shown in Table 8, indicating that monthly averaging of the data before computing S_A smooths the unwanted synoptic variablity. The rate of energy storage is generally less then 20 W m^{-2} and plays a small role in the monthly energy budget. Thus, the method used to obtain S_A should not greatly alter the overall energy balance.

The atmospheric flux divergence of energy, div F_A, presented in Tables 9-11, includes the contributions of both the mean and eddy fluxes. Div F_A is an important component of the atmospheric energy balance having the same order of magnitude as the net radiation. Positive values indicate a divergence or export of energy from a region while negative values signify energy convergence or import. The values obtained for div F_A from regions 1-5 indicate energy export from oceanic to continental regions during the Northern Hemisphere winter. This process occurs in response to the

TABLE 8. The rate of energy stored in the atmosphere (W m^{-2}) during the month of June computed by taking the difference between the average July and May energy stored in the air colomn Using diagnostics from the GLA pressure model. Also given are the rate of energy stored during june for 10 latitude bands in the Northern Hemisphere as calculated by Oort and Vonder Haar (1976).

GLA Pressure Model				Oort and Vander Haar	
Region	Latitude	Longitude	June S_A	Latitude Band	June S_A
27	8S-12N	47.5W- 7.5W	-4.9	0-10N	-3.1
28	8S-12N	117.5E- 82.5W	-3.1	10N-20N	1.6
29	8S-12N	47.5E-112.5E	-2.3	20N-30N	9.0
30	12N-32N	87.5W- 17.5W	6.9	30N-40N	16.1
31	12N-32N	112.5E-112.5W	7.1	40N-50N	17.0
32	32N-52N	72.5W- 7.5W	13.5	50N-60N	17.3
33	32N-52N	132.5E-122.5W	18.3	60N-70N	18.7
34	52N-72N	37.5W- 7.5E	15.8	70N-80N	19.1

TABLE 9. Flux divergence of energy within the atmosphere (W m^{-2})

Region	Latitude	Longitude	Location	Jan	Feb	Jan-Feb	May	June	July	May-July
1	20N-60N	72.5W- 12.5W	N. Atlantic	29	106	65	-19	-30	-38	-31
2	28N-60N	122.5W- 72.5W	N. America	-70	-99	-83	19	54	47	41
3	20N-60N	137.5E-122.5W	N. Pacific	66	37	52	-40	-43	-45	-44
4	24N-60N	12.5W-137.5E	Eurasia	-28	-17	-22	21	36	34	31
5	44N-68N	7.5W- 37.5E	Europe	-63	-76	-69	13	77	35	45
6	12N-32N	97.5W- 62.5W	Caribbean	74	102	87	36	23	72	42
7	8N-32N	17.5W- 47.5E	N. Africa	-5	21	8	56	51	70	59
8	32S- 8N	12.5E- 37.5E	S. Africa	49	44	47	-12	-1	-30	-15
9	36S- 8N	72.5W- 47.5W	S. America	56	35	46	-4	-3	5	-2
10	36S-16S	112.5E-152.5E	Australia	36	3	20	-22	-19	15	-9

TABLE 10. Flux divergence of energy within the atmosphere ($W\ m^{-2}$)

Region	Latitude	Longitude	Location	Jan	Feb	Jan-Feb	May	June	July	May-July
11	68S-36S	67.5W- 77.5W	Antarctic O.	-21	-24	-23	-9	-6	-13	-9
12	36S- 4S	42.5W- 12.5E	Atlantic O.	19	32	26	-5	-14	-12	-9
13	36S- 4S	152.5E- 77.5W	Pacific O.	23	31	27	40	23	35	33
14	36S- 4S	37.5E-112.5E	Indian O.	26	37	32	39	5	-22	9
15	4S-28N	57.5W- 17.5W	Atlantic O.	50	40	45	32	32	27	31
16	4S-28N	107.5E-107.5W	Pacific O.	65	55	60	52	51	41	47
17	28N-60N	72.5W- 7.5W	Atlantic O.	5	109	54	-54	-68	-84	-71
18	28N-60N	142.5E-127.5W	Pacific O.	24	9	17	-87	-89	-101	-94
19	60N-80N	27.5W- 17.5E	Atlantic O.	20	-76	-25	-62	-164	-218	-144

TABLE 11. Flux divergence of energy within the atmosphere (W m^{-2})

Region	Latitude	Longitude	Location	Jan	Feb	Jan-Feb	May	June	July	May-July
20	68S-48S	Continous band	Antarctic O.	-18	-30	-24	-16	4	-11	-8
21	48S-28S	52.5W- 17.5E	Atlantic O.	-20	7	-6	-17	-18	-41	-27
22	48S-28S	147.5E- 77.5W	Pacific O.	-12	-8	-10	12	-15	7	2
23	48S-28S	22.5E-117.5E	Indian O.	-6	2	-2	-4	-6	18	4
24	28S- 8S	42.5W- 12.5E	Atlantic O.	17	46	31	-3	-30	-13	-15
25	28S- 8S	147.5E- 77.5W	Pacific O.	25	32	28	51	22	26	33
26	28S- 8S	37.5E-112.5E	Indian O.	34	29	32	44	1	-40	4
27	8S-12N	47.5W- 7.5W	Atlantic O.	40	10	25	24	57	35	39
28	8S-12N	117.5E- 82.5W	Pacific O.	44	26	35	46	40	34	40
29	8S-12N	47.5E-112.5E	Indian O.	37	55	45	81	109	86	91
30	12N-32N	87.5W- 17.5W	Atlantic O.	49	76	62	15	-9	30	11
31	12N-32N	112.5E-112.5W	Pacific O.	74	67	70	36	33	23	30
32	32N-52N	72.5W- 7.5W	Atlantic O.	18	112	62	-62	-90	-108	-88
33	32N-52N	132.5E-122.5W	Pacific O.	76	24	51	-78	-106	-119	-103
34	52N-72N	37.5W- 7.5E	Indian O.	-23	-45	-32	-33	-73	-118	-75

differential heating characteristics of water and land. During winter the oceans, which have retained more of the energy they received during summer than has land, release large amounts of heat to the atmosphere via fluxes of sensible and latent heat (Table 17). Some of this energy is exported to the continents which are heat sinks in winter. Due to their small heat capacity and shallow layer of heating, continents gain heat more rapidly and reach a higher temperature than the oceans during spring and summer. This energy is imparted to the overlying air which transports it to oceanic regions. The land areas in the Southern Hemisphere (regions 8-10) also exhibit this climatic regime. However, div F_A over oceanic sections south of the equator tend to be small and indicate export in the meridional direction rather than strong zonal land-sea exchanges. This is probably caused by the limited land mass between $20^{o}S$-$70^{o}S$.

Several recent studies have obtained regional estimates of div F_A and its components, the kinetic energy, sensible heat, geopotential energy and latent heat. Swinbank (1983) calculated the divergence terms from the British Meteorological Office FGGE IIIa analysis (Lyne et al. 1982) and from European Center For Medium Range Weather Forecasts IIIb analysis (Bengtsson et al. 1982), which in the following we respectively refer to as the Met Office and ECMWF analyses. The Met Office and ECMWF assimilation systems have been described and compared by Hollingsworth (1985a) for synoptic forecasts and by Lorenc and Swinbank (1984) with respect to producing general circulation statistics. The results from our study

which used the GLA IIIb pressure analysis are given with Swinbank's in Table 12 for July 1979. The values are presented for the North Atlantic, North America, North Pacific and Eurasian sectors both before and after the mass balance correction has been applied.

The results of these studies show that the sensible and geopotential energy divergences tend to compensate one another, having the same magnitude but opposite sign. This balance has been attributed to a thermally direct circulation (Alestalo, 1981; White and Saltzman, 1956). A rising air parcel cools adiabatically, decreasing its internal energy while gaining potential energy, whereas the opposite occurs in subsiding air. The relation between the vertical motion and the flux divergence of the two energies can be seen by vertically integrating and then equating the kinetic and sensible energy equations (Eqs. (4) & (6) in Appendix I)

$$\int_{50}^{P_S} \frac{\partial K}{\partial t}\, dp/g + \int_{50}^{P_S} \nabla\cdot(K + gz)\vec{V}\, dp/g - \int_{50}^{P_S} \vec{V}\cdot\vec{F}\, dp/g = -\omega\alpha \tag{21}$$

$$= -\int_{50}^{PS} c_p \frac{\partial T}{\partial t}\, dp/g - \int_{50}^{P_S} \nabla\cdot c_p T\vec{V}\, dp/g + \int_{50}^{P_S} S\, dp/g$$

The two equations are linked via the vertical motion term ($\omega\alpha$) which responds to both thermal and mechanical forcing. As discussed previously, the storage terms, the frictional dissipation and the flux divergence of kinetic energy are all relatively small. The diabatic heating (the final term on the right hand side) is zero in an adiabatic process and thus

TABLE 12. The uncorrected and mass-corrected atmospheric energy flux divergence (W m^{-2}) for regions 1-4, during July 1979 as given by the British Meterological Office, ECMWF (Swinbank, 1983) and by the GLA pressure diagnostics.

	Sensible		Geopotential		Latent		Total	
	uncor	corr	uncor	corr	uncor	corr	uncor	corr
North Atlantic								
British Met	159	66	-89	-109	17	14	88	-32
ECMWF	149	41	-96	-80	11	14	64	-26
GLA Pressure	-25	56	-124	-103	5	7	-143	-38
North America								
British Met	-54	-11	30	40	6	7	-19	37
ECMWF	-40	-20	36	40	5	4	1	25
GLA Pressure	278	45	46	-14	24	16	348	47
North Pacific								
British Met	127	-30	38	3	-13	-19	153	-46
ECMWF	-44	-22	-14	-9	-24	-24	-83	-54
GLA Pressure	-303	-85	21	75	-43	-35	-325	-45
EURASIA								
British Met	20	40	-9	-4	-8	-7	3	29
ECMWF	-107	42	8	-10	-9	-12	-108	21
GLA Pressure	85	66	-35	-41	9	10	58	34

$$\int_{50}^{P_S} \nabla\cdot gz\vec{V}\, dp/g \sim - \int_{50}^{P_S} \nabla\cdot c_p T\vec{V}\, dp/g \qquad (22)$$

As noted in section 4C a correction is applied to the flux divergence to ensure mass conservation in the budget column. Using radiosonde data from 1974-1976, Alestalo (1981) found that in the annual mean, mass divergence leads to a decrease in the surface pressure of approximately 18 mb/day over Europe, which he attributed to sub-synoptic scale flow between the surface and 850 mb. Diagnostics generated by the GLA analysis also have this flaw, with long-term mean surface pressure changes of about 5 mb/day. Burridge (1985) estimated that even a 1 mb/day bias in the surface pressure would result in the correction of div F_A by approximately 40 W m^{-2}. This clearly demonstrates the necessity of mass balance corrections. Table 12 shows that the corrections are as large or even larger than the uncorrected values of the flux divergence of sensible and geopotential energy, while insignificant for latent and kinetic energy.

The atmospheric energy flux divergence is a difficult quantity to determine as it is computed from the difference between large numbers. To investigate the accuracy of div F_A and its components the results using the Met Office, ECMWF and GLA analyses are contrasted in Table 12. After the mass balance correction has been applied, there is fairly good agreement between the three estimates of the flux divergence of each energy component over the Atlantic. In the other three regions large differences occur between the

estimates of sensible and geopotential flux divergence. For example, over North America the GLA values indicate sensible heat divergence and geopotential energy convergence, results which are in contrast to the Met Office and ECMWF analyses. Over the continents in summer, one would expect export of geopotential energy associated with low level inflow, rising motion, and upper level outflow. The explanation for the apparently inconsistent results given by the GLA analysis is not clear. When the sensible and geopotential energies are considered together the differences between studies are substantially reduced, causing the total energy flux divergence estimates to differ by less than 20 W m^{-2}.

Table 13 presents the atmospheric energy flux divergence for winter and summer as computed by Burridge (see Bretherton, et al. 1982), Alestalo (1981) and the present study. Burridge utilized ECMWF FGGE IIIb analysis for areas approximating each of the Northern Hemisphere continents and oceans while Alestalo investigated the energy balance over Europe. While our regions and time periods are not exactly coincident with those used by Alestalo and Burridge, they are reasonably close, allowing for a rough comparison between results.

The flux divergence of kinetic energy is small compared with the other three energies, as shown in Table 13. As with the first set of comparisons, large differences are found between the estimates of sensible and geopotential energy divergence but a balance between the two leads to values of div F_A which differ by approximately 20-30 W m^{-2}. The exception is the summer value of div

TABLE 13. The atmospheric energy flux divergence for North Atlantic, North America, North Pacific and Eurasia ($W\ m^{-2}$) as computed by Burridge for the "CAGE" Experiment: a Feasibility Study. The atmospheric flux divergence for Europe as computed by Alestalo (1981) during 1974-1976 and the energy divergence results of GLA Pressure model during SOP I & II.

Region	Study	Kinetic	Sensible	Geopotential	Latent	Total
			Winter			
N. Atlantic	Burridge	-6	68	-16	36	81
	GLA Pressure	-7	123	-92	40	65
N. America	Burridge	7	2	-33	-37	-61
	GLA Pressure	10	-25	-32	-36	-83
N. Pacific	Burridge	-3	16	33	10	24
	GLA Pressure	-7	14	31	15	52
Eurasia	Burridge	3	87	-80	-11	-1
	GLA Pressure	4	107	-136	3	-22
Europe	Alestalo	-10	-88	39	-33	-92
	GLA Pressure	-1	-109	80	-40	-69
			Summer			
N. Atlantic	Burridge	0	39	-65	11	-15
	GLA Pressure	0	59	-105	15	-31
N. America	Burridge	0	-17	11	1	-5
	GLA Pressure	-1	80	-47	9	41
N. Pacific	Burridge	0	-81	48	-34	-66
	GLA Pressure	0	-65	43	-22	-44
Eurasia	Burridge	0	33	9	1	43
	GLA Pressure	0	79	-62	14	30
Europe	Alestalo	-3	14	-2	6	15
	GLA Pressure	-3	64	-45	28	45

F_A for North America; Burridge obtained a value of -5 W m^{-2}, contrasted with 41 W m^{-2} computed using the GLA analysis. The latter value appears to be more realistic as it is in better agreement with the July estimates of div F_A over the North Atlantic given in Table 12. Additionally, one would expect an export of energy from the North American Continent in the summer as part of the land-sea energy balance described previously.

The net flux of energy at the earth-atmosphere interface, F_S, (Tables 14-16) includes the surface sensible, latent heat and radiative flux as indicated by Eq. (10). In the extratropics, there is a substantial transfer of energy from the ocean to the atmosphere ($F_S < 0$) during winter and a larger summer air-to-sea transfer. One would expect the winter F_S values to be of greater magnitude than their summer counterparts, as was found by Lamb and Bunker (1982) for the Atlantic and by Esbensen and Kushnir (1981) for the global oceans. The seasonal bias in our results can be attributed to the GLA model producing excess shortwave radiation absorption at the earth's surface (as described previously in this section), causing winter F_S values to be less negative and summer values more positive. The longwave and convective flux values compare reasonably well with estimates obtained from the atlas of Esbensen and Kushnir (1981).

The surface fluxes over land also show that energy is transfered from surface to air during winter and in the opposite direction in summer. The rate at which energy is stored by land is estimated to be small, with monthly values generally less then 5

TABLE 14. Energy flow from the atmosphere to the earth (W m^{-2})

Region	Latitude	Longitude	Location	Jan	Feb	Jan-Feb	May	June	July	May-July
1	20N-60N	72.5W- 12.5W	N. Atlantic	-122	-137	-128	133	165	158	153
2	28N-60N	122.5W- 72.5W	N. America	-38	31	-7	48	47	36	40
3	20N-60N	137.5E-122.5W	N. Pacific	-151	-74	-115	151	183	172	168
4	24N-60N	12.5W-137.5E	Eurasia	-59	-31	-45	62	54	50	57
5	44N-68N	7.5W- 37.5E	Europe	-103	-48	-77	11	3	24	14
6	12N-32N	97.5W- 62.5W	Caribbean	-120	-77	-100	58	71	31	53
7	8N-32N	17.5W- 47.5E	N. Africa	-19	-13	-16	27	35	13	28
8	32S- 8N	12.5E- 37.5E	S. Africa	21	39	30	52	26	45	43
9	36S- 8N	72.5W- 47.5W	S. America	23	41	32	33	8	10	19
10	36S-16S	112.5E-152.5E	Australia	76	74	75	19	-27	-48	-18

TABLE 15. Energy flow from the atmosphere to the earth (W m^{-2})

Region	Latitude	Longitude	Location	Jan	Feb	Jan-Feb	May	June	July	May-July
11	68S-36S	67.5W- 77.5W	Antarctic O.	156	102	130	-118	-133	-132	-127
12	36S- 4S	42.5W- 12.5E	Atlantic O.	113	86	102	19	2	3	9
13	36S- 4S	152.5E- 77.5W	Pacific O.	94	89	90	-19	-35	-37	-32
14	36S- 4S	37.5E-112.5E	Indian O.	81	62	73	-23	-35	1	-18
15	4S-28N	57.5W- 17.5W	Atlantic O.	-37	4	-16	71	78	76	76
16	4S-28N	107.5E-107.5W	Pacific O.	-49	-5	-28	54	48	66	55
17	28N-60N	72.5W- 7.5W	Atlantic O.	-132	-166	-147	162	202	201	190
18	28N-60N	142.5E-127.5W	Pacific O.	-143	-74	-111	191	240	232	220
19	60N-80N	27.5W- 17.5E	Atlantic O.	-196	-96	-149	67	229	254	179

TABLE 16. Energy flow from the atmosphere to the earth (W m^{-2})

Region	Latitude	Longitude	Location	Jan	Feb	Jan-Feb	May	June	July	May-July
20	68S-48S	Continous band	Antarctic O.	139	82	112	-136	-162	-153	-150
21	48S-28S	52.5W- 17.5E	Atlantic O.	168	109	141	-56	-66	-68	-63
22	48S-28S	147.5E- 77.5W	Pacific O.	160	127	142	-88	-84	-104	-94
23	48S-28S	22.5E-117.5E	Indian O.	161	100	134	-68	-103	-116	-95
24	28S- 8S	42.5W- 12.5E	Atlantic O.	113	69	93	31	22	14	24
25	28S- 8S	147.5E- 77.5W	Pacific O.	87	85	84	-18	-26	-17	-21
26	28S- 8S	37.5E-112.5E	Indian O.	67	67	68	-15	-26	24	-5
27	8S-12N	47.5W- 7.5W	Atlantic O.	3	51	27	31	17	35	29
28	8S-12N	117.5E- 82.5W	Pacific O.	4	50	24	39	28	48	37
29	8S-12N	47.5E-112.5E	Indian O.	-1	31	15	-6	-28	-20	-15
30	12N-32N	87.5W- 17.5W	Atlantic O.	-81	-48	-65	113	138	96	117
31	12N-32N	112.5E-112.5W	Pacific O.	-94	-43	-71	95	98	111	100
32	32N-52N	72.5W- 7.5W	Atlantic O.	-140	-174	-155	173	226	231	210
33	32N-52N	132.5E-122.5W	Pacific O.	-191	-79	-139	187	257	251	232
34	52N-72N	37.5W- 7.5E	Atlantic O.	-151	-92	-124	84	186	193	155

W m^{-2} (Gabites, 1950). This would require the net flux of energy across the land-air interface also to be small. The values obtained for F_S over land, though generally one fourth to one half as large as ocean surface fluxes in the same latitude belt, may be excessive. Many of the continental regions include small sections of ocean (see Figs. 3-5). The substantial flux of latent heat in these sections may partly explain why the magnitude of F_S over land is larger than expected.

The surface convective flux (SH + LH) is obtained as a residual from the atmospheric energy budget and can be analyzed independently of F_S. The monthly averaged results presented in Table 17 (the seasonal results are shown in Table 27) indicate that convective fluxes transfer energy almost exclusively from the earth to the atmosphere. These fluxes are strongest for regions located between $10^{o}N$-$50^{o}N$, with winter values exceeding 200 W m^{-2} over the oceans. During this time of year cold continental air often flows over the warm waters of the Kuroshio Current and the Gulf Stream, respectively located in the northwest Pacific and Atlantic Oceans. The resulting unstable vertical profiles of atmospheric temperature lead to strong turbulent mixing and consequently large upward fluxes of sensible and latent heat. Esbensen and Kushnir (1981) have shown that in January and February both the upward sensible and latent heat fluxes are maximized along the western boundaries of the Atlantic and Pacific Oceans. In summer, the large earth-to-atmosphere fluxes relocate over the continents as the land surfaces become warmer than the surrounding oceans. The seasonal and

TABLE 17. The flux of sensible plus latent heat from the earth to the atmosphere (W m^{-2}).

Reg	Latitude	Longitude	Location	Jan	Feb	May	June	July
Climatic Regions								
1	20N-60N	72.5W- 12.5W	N. Atlantic	177	227	90	83	87
2	28N-60N	122.5W- 72.5W	N. America	59	26	130	156	159
3	20N-60N	137.5E-122.5W	N. Pacific	205	166	75	71	82
4	24N-60N	12.5W-137.5E	Eurasia	89	92	120	140	139
5	44N-68N	7.5W- 37.5W	Europe	90	60	138	168	144
6	12N-32N	97.5W- 62.5W	Caribbean	240	230	154	142	177
7	8N-32N	17.5W- 47.5E	N. Africa	108	127	154	147	170
8	32S- 8N	12.5E- 37.5E	S. Africa	158	138	101	108	95
9	36S- 8N	72.5W- 47.5W	S. America	164	138	103	121	126
10	36S-16S	112.5E-152.5E	Australia	139	117	90	115	138
32^{o} Ocean Segments								
11	68S-36S	67.5W- 77.5W	Antarctic O	85	89	136	133	136
12	36S- 4S	42.5W- 12.5E	Atlantic O	137	155	133	122	124
13	36S- 4S	152.5E- 77.5W	Pacific O	139	145	165	157	167
14	36S- 4S	37.5E-112.5E	Indian O	154	157	165	155	123
15	4S-28N	57.5W- 17.5W	Atlantic O	189	175	155	146	155
16	4S-28N	107.5E-107.5W	Pacific O	197	178	159	168	155
17	28N-60N	72.5W- 7.5W	Atlantic O	156	228	54	48	45
18	28N-60N	142.5E-127.5W	Pacific O	168	137	26	18	26
19	60N-80N	27.5W- 17.5E	Atlantic O	143	62	30	-86	-117
20^{o} Ocean Segments								
20	68S-48S	Continous band	Antarctic O	87	85	130	142	137
21	48S-28S	52.5W- 17.5E	Atlantic O	91	115	123	108	112
22	48S-28S	147.5E- 77.5W	Pacific O	99	96	152	123	148
23	48S-28S	22.5E-117.5E	Indian O	100	128	133	142	158
24	28S- 8S	42.5W- 12.5E	Atlantic O	138	174	133	111	122
25	28S- 8S	147.5E- 77.5W	Pacific O	140	148	174	159	158
26	28S- 8S	37.5E-112.5E	Indian O	168	152	170	158	111
27	8S-12N	47.5W- 7.5W	Atlantic O	181	147	163	169	166
28	8S-12N	117.5E- 82.5W	Pacific O	176	141	153	159	146
29	8S-12N	47.5E-112.5E	Indian O	171	156	199	205	205
30	12N-32N	87.5W- 17.5W	Atlantic O	202	203	128	111	149
31	12N-32N	112.5E-112.5W	Pacific O	208	198	146	154	145
32	32N-52N	72.5W- 7.5W	Atlantic O	168	237	50	31	24
33	32N-52N	132.5E-122.5W	Pacific O	219	147	36	5	12
34	52N-72N	37.5W- 7.5E	Atlantic O	108	83	70	16	1

land-ocean differences in SH + LH in the Southern Hemisphere are damped by the large expanses of ocean which tend to reduce the variability of air-earth temperature and moisture differences.

B. The oceanic budget

The energy balance for the ocean regions is given by Eq. (13), which indicates a balance between the net energy passing through the ocean surface, F_S, the rate at which energy is stored within the oceans, S_O, and the divergence of energy from the regions via currents, div F_O. Our intent here is not to obtain the most precise estimates of the budget terms, but rather to examine their physical consistency, accuracy and sensitivity to errors.

In the oceans, the geopotential and pressure work terms essentially compensate each other and the kinetic energy is extremely small, thus only the sensible energy needs to be considered. Some of the ocean regions include land or ice. The change in the heat stored by land has been shown to be small (Gabites, 1950), while the effects of flow, formation and melting of ice are not well known. From measurements of Aagaard and Greisman (1975) and "tentative" model calculations of Oort and Vonder Haar (1976), the seasonal changes in the energy stored by ice appear to be less then 15 W m^{-2}, though ice could play an important role in the local energy balance of the polar oceans.

The depth to which the annual cycle affects the heat storage varies with location and time of year. In most ocean basins significant changes in S_O are confined to the top 200 m, but in some

locations vertical mixing can occur over great depths and seasonal changes in temperature are noticeable down to 1000 m (Levitus, 1984). Oort and Vonder Haar (1976) chose 275 m as a lower limit of integration, as they determined that the month-to-month variations below this depth were small and possibly unreliable. Lamb and Bunker (1982) measured ocean heat storage to depths of 300 and 500 m and found the results to be significantly different in some instances.

To examine how the choice of a lower boundary impacts S_0, the sensible heat in the water column is integrated from the surface to 250, 500 and 1000 m depth, with the results shown in Table 18. The differences between these three integrations are surprisingly large and somewhat suspect in the Atlantic and Indian Oceans between 28^{o}-48^{o}S. However, Levitus (1984) found relatively large interannual temperature changes, down to 1000 m depth for both of these regions. The remainder of the regions showed differences which were smaller though not insignificant, with the three estimates of S_0 generally deviating by 40 W m^{-2} or less.

It is difficult to separate the actual variation of heat storage with depth from the variations caused by data deficiencies. Many of the ocean casts do not extend to 1000 m; there are nearly 1.5 million global observations at the surface but less then 100,000 at 1 km. The ratio of the number of measurements at 250, 500, 1000 m is respectively 8.9:1.6:1 (Levitus, 1982). In addition, there is a general lack of data south of 20^{o}S. Assuming the data at greater depths are reasonable, the values of S_0 used in the budget analysis are computed by integrating the sensible heat from the surface to

Table 18. Energy stored in the oceans (W m^{-2}) obtained by integrating the sensible heat from the surface to depths of 250 m, 500 m, and 1000 m.

Region	Latitude	Longitude	Ocean	January 250m	January 500m	January 1000m	July 250m	July 500m	July 1000m
32^{o} Ocean Segments									
11	68S-36S	67.5W- 77.5W	Antarctic	73	70	85	-39	-16	12
12	36S- 4S	42.5W- 12.5E	Atlantic	35	27	34	-48	6	4
13	36S- 4S	152.5E- 77.5W	Pacific	89	75	59	-59	-42	-61
14	36S- 4S	37.5E-112.5E	Indian	38	23	15	36	61	75
15	4S-28N	57.5W- 17.5W	Atlantic	-82	-92	-104	59	48	45
16	4S-28N	107.5E-107.5W	Pacific	-63	-70	-88	28	22	9
17	28N-60N	72.5W- 7.5W	Atlantic	-141	-141	-136	133	138	158
18	28N-60N	142.5E-127.5W	Pacific	-174	-172	-173	127	113	125
19	60N-80N	27.5W- 17.5E	Atlantic	-91	-116	-134	96	115	121
20^{o} Ocean Segments									
20	68S-48S	Continous band	Antarctic	62	45	12	-64	-77	-60
21	48S-28S	52.5W- 17.5E	Atlantic	10	-60	-116	97	305	368
22	48S-28S	147.5E- 77.5W	Pacific	178	198	208	-93	-114	-156
23	48S-28S	22.5E-117.5E	Indian	86	158	329	-16	32	66
24	28S- 8S	42.5W- 12.5E	Atlantic	18	4	9	-77	-68	-69
25	28S- 8S	147.5E- 77.5W	Pacific	60	38	17	-48	-18	-38
26	28S- 8S	37.5E-112.5E	Indian	12	-6	-30	49	67	80
27	8S-12N	47.5W- 7.5W	Atlantic	-67	-74	-56	29	22	18
28	8S-12N	117.5E- 82.5W	Pacific	-36	-50	-77	-4	-7	-16
29	8S-12N	47.5E-112.5E	Indian	47	55	71	-26	-15	18
30	12N-32N	87.5W- 17.5W	Atlantic	-107	-105	-111	61	43	37
31	12N-32N	112.5E-112.5W	Pacific	-89	-83	-85	56	46	46
32	32N-52N	72.5W- 7.5W	Atlantic	-155	-150	-136	139	147	188
33	32N-52N	132.5E-122.5W	Pacific	-181	-178	-176	134	115	119
34	52N-72N	37.5W- 7.5E	Atlantic	-76	-73	-88	112	129	130

1000 m, in order to maximize the information available.

The mean monthly and seasonal values of S_0 are given for January, February and May through July in Tables 19 and 20 for the 32^o and 20^o ocean segments (regions 11-34). In general, they indicate an accumulation of energy in the summer months and energy loss during winter in the extratropics. The maximum and minimum values of S_0 occur between 30^o-50^o in both hemispheres. The magnitude of S_0 in the tropics tends to be larger than F_S, indicating that heat is either being advected through the side boundaries by currents and/or through the lower boundary via upwelling and downwelling. In the equatorial oceans, both horizontal and vertical motions are associated with the wind driven Ekman flow and baroclinic Kelvin waves (Levitus, 1982; Gill, 1982). The features of S_0 described above are consistent with the work of Levitus (1984), Oort and Vonder Haar (1976), and Lamb and Bunker (1982).

The ocean heat flux divergence, div F_0, is calculated as a residual from Eq. (13), ie. S_0 minus F_S. These two terms are computed with different data sets. F_S is derived from five months of data in 1979 while while S_0 is calculated from a historical record spanning 70 years. Thus the values obtained for div F_0, while useful for investigating the characteristics of the ocean energy divergence, are not representative of the climatic mean state. Tables 21 and 22 show that div F_0 is the same order of magnitude as the ocean storage and surface flux terms and therefore plays an important role in the earth's energy balance. Oort and Vonder Haar

TABLE 19. Time rate of change of energy stored in the oceans ($W\ m^{-2}$).

Region	Latitude	Longitude	Ocean	Jan	Feb	Jan-Feb	May	June	July	May-July
11	68S-36S	67.5W- 77.5W	Antarctic	85	51	68	-182	-39	12	-70
12	36S- 4S	42.5W- 12.5E	Atlantic	34	14	24	-136	-66	4	-66
13	36S- 4S	152.5E- 77.5W	Pacific	59	-42	10	-48	-157	-61	-89
14	36S- 4S	37.5E-112.5E	Indian	15	-18	-1	-134	-103	75	-54
15	4S-28N	57.5W- 17.5W	Atlantic	-104	-13	-59	56	83	45	61
16	4S-28N	107.5E-107.5W	Pacific	-88	35	-28	31	-1	9	13
17	28N-60N	72.5W- 7.5W	Atlantic	-136	-57	-97	127	131	158	139
18	28N-60N	142.5E-127.5W	Pacific	-173	-139	-156	129	144	125	132
19	60N-80N	27.5W- 17.5E	Atlantic	-134	-247	-189	152	132	121	135

TABLE 20. Time rate of change of energy stored in the oceans (W m^{-2})

Region	Latitude	Longitude	Ocean	Jan	Feb	Jan-Feb	May	June	July	May-July
20	68S-48S	Continous band	Antarctic	12	79	45	-152	-106	-60	-106
21	48S-28S	52.5W- 17.5E	Atlantic	-116	-106	-111	-439	-158	368	-75
22	48S-28S	147.5E- 77.5W	Pacific	208	40	125	-163	-87	-156	-135
23	48S-28S	22.5E-117.5E	Indian	329	67	201	-161	142	66	16
24	28S- 8S	42.5W- 12.5E	Atlantic	9	28	18	-9	10	-69	-23
25	28S- 8S	147.5E- 77.5W	Pacific	17	-95	-37	-4	-156	-38	-66
26	28S- 8S	37.5E-112.5E	Indian	-30	-77	-52	-137	-105	80	-54
27	8S-12N	47.5W- 7.5W	Atlantic	-56	-29	-43	30	87	18	45
28	8S-12N	117.5E- 82.5W	Pacific	-77	34	-23	-17	-65	-16	-32
29	8S-12N	47.5E-112.5E	Indian	71	79	74	-29	-31	18	-14
30	12N-32N	87.5W- 17.5W	Atlantic	-111	-13	-63	92	84	37	71
31	12N-32N	112.5E-112.5W	Pacific	-85	17	-35	69	43	46	53
32	32N-52N	72.5W- 7.5W	Atlantic	-136	-111	-124	145	138	188	157
33	32N-52N	132.5E-122.5W	Pacific	-176	-164	-170	116	163	119	132
34	52N-72N	37.5W- 7.5E	Atlantic	-88	25	-33	136	113	130	127

TABLE 21. Flux divergence of energy within the oceans (W m^{-2}).

Region	Latitude	Longitude	Ocean	Jan	Feb	Jan-Feb	May	June	July	May-July
11	68S-36S	67.5W- 77.5W	Antarctic	72	50	62	64	-93	-144	-58
12	36S- 4S	42.5W- 12.5E	Atlantic	79	72	77	155	68	-1	75
13	36S- 4S	152.5E- 77.5W	Pacific	36	131	80	28	122	25	57
14	36S- 4S	37.5E-112.5E	Indian	66	80	74	112	68	-74	36
15	4S-28N	57.5W- 17.5W	Atlantic	66	17	43	15	-5	31	14
16	4S-28N	107.5E-107.5W	Pacific	40	-39	0	23	49	57	42
17	28N-60N	72.5W- 7.5W	Atlantic	4	-109	-50	36	71	43	51
18	28N-60N	142.5E-127.5W	Pacific	30	65	45	63	96	107	88
19	60N-80N	27.5W- 17.5E	Atlantic	-62	151	40	-85	97	133	44

TABLE 22. Flux divergence of energy within the ocean (W m^{-2}).

Region	Latitude	Longitude	Ocean	Jan	Feb	Jan-Feb	May	June	July	May-July
20	68S-48S	Continous band	Antarctic	126	3	67	16	-56	-93	-44
21	48S-28S	52.5W- 17.5E	Atlantic	284	216	252	383	92	-436	12
22	48S-28S	147.5E- 77.5W	Pacific	-48	88	17	75	3	52	42
23	48S-28S	22.5E-117.5E	Indian	-169	34	-67	93	-245	-182	-111
24	28S- 8S	42.5W- 12.5E	Atlantic	104	41	75	40	12	83	47
25	28S- 8S	147.5E- 77.5W	Pacific	70	180	122	-14	130	21	45
26	28S- 8S	37.5E-112.5E	Indian	96	144	120	122	79	-56	49
27	8S-12N	47.5W- 7.5W	Atlantic	59	80	70	1	-71	17	-17
28	8S-12N	117.5E- 82.5W	Pacific	81	16	47	56	93	63	70
29	8S-12N	47.5E-112.5E	Indian	-71	-48	-59	22	3	-38	1
30	12N-32N	87.5W- 17.5W	Atlantic	29	-35	-2	21	54	59	46
31	12N-32N	112.5E-112.5W	Pacific	-9	-61	-36	27	55	64	47
32	32N-52N	72.5W- 7.5W	Atlantic	-4	-62	-31	28	89	43	53
33	32N-52N	132.5E-122.5W	Pacific	-15	85	31	71	95	133	100
34	52N-72N	37.5W- 7.5E	Atlantic	-64	-117	-91	-53	73	62	28

(1976) found strong heat convergence during the Northern Hemisphere winter between 45^{o}N-60^{o}N, a result apparent in our work. The exception to this finding is the heat divergence found in the North Pacific (region 33) during February. Heat import into this latitude belt during the Northern Hemisphere summer was shown to occur in the Atlantic by Lamb and Bunker (1982) and for the global oceans by Oort and Vonder Haar, in contrast to this study. In the tropics our results show that the Atlantic and Pacific (regions 27 and 28) tend to export heat for the months of January and February while heat is imported into the Indian Ocean (region 29). Overall, there is a net export of heat from the tropical oceans in each of the five months presented, in agreement with Oort and Vonder Haar (1976). Some of the values obtained for div F_0 in the Southern Hemisphere are suspect, especially in the South Atlantic and Indian Oceans. In addition, heat is exported from the oceans surrounding Antarctica during January, February and May, a result which seems physically unrealistic. These questionable features are likely due to a paucity of data in both the atmosphere and ocean in the Southern Hemisphere.

C. Ocean heat transport

The vertically integrated meridional ocean heat transport, F_0, is obtained by a southward summation of $\langle \text{div } F_0 \rangle A$ with the assumption of a boundary condition at the poleward edge of the northernmost region. Lamb and Bunker (1982) adopted values of F_0 from Aagard and Greisman (1975) for their boundary value at 70^{o}N. The meridional heat transport in the Arctic Ocean appears to be

nearly zero and occurs mainly in the Norwegian Sea (Aagard and Greisman, 1975; Vowinckel and Orvig 1970). Therefore, the values of F_S given by Lamb and Bunker (1982) at 70°N in the Atlantic Ocean are used as the northern boundary values for both the 32° and 20° ocean segments, located respectively at 80°N and 72°N. The summation procedure used to compute F_0 compounds inaccuracies, causing the values of the meridional heat transport to be less reliable the more southerly the latitude.

The values of F_0 for the combined contributions of all oceans are presented in Table 23. In Table 24 the results of this study are shown with those of Lamb and Bunker (1982) for the Atlantic Ocean. Both tables are given in units of petawatts (10^{15} watts). The accumulation of error in F_0 with southward integration is manifested in the maximum negative values occuring at 68°S. This latitude is very near the Antarctic coast where F_0 should approach zero. The negative bias may be attributed to an overestimation of the solar radiation absorbed at the surface, which in turn leads to larger values of div F_0 and more negative values of F_0. The bias is greatest when the shortwave flux is a maximum causing the values of F_0 in the Northern Hemisphere to be more accurate in winter than summer. This discrepancy also appears when comparing the results of the present study to those of Oort and Vonder Haar (1976), and Lamb and Bunker (1982).

The values of F_0 obtained using the 32° and 20° bands are generally consistent with each other, though they differ north of the equator for the months of January and February. For this time

TABLE 23. Oceanic heat transport (10^{15} W) as given by the 32^{o} and 20^{o} bands.

	Latitude	Jan	Feb	Jan-Feb	May	June	July	May-July
32 Bands								
	80N	.1	.1	.1	.1	.1	.2	.1
	60N	.3	-.7	-.1	.5	-.4	-.5	-.1
	28N	-.5	-.4	-.4	-1.7	-4.2	-4.0	-3.3
	4S	-3.7	1.6	-1.0	-3.2	-6.8	-7.7	-5.8
	36S	-8.8	-7.3	-7.5	-7.9	-15.0	-7.7	-9.0
	68S	-14.8	-11.6	-12.7	-13.2	-7.2	4.4	-4.1
20 Bands								
	72N	.1	.1	.1	.1	.1	.2	.1
	52N	.4	.7	.6	.3	-.3	-.2	0.0
	32N	.7	-.2	.3	-1.3	-3.2	-3.2	-2.6
	12N	.6	2.2	1.8	-2.5	-5.8	-6.1	-3.4
	8S	-2.1	1.5	.2	-5.0	-8.8	-8.2	-5.9
	28S	-7.3	-7.2	-6.7	-7.3	-14.4	-8.9	-8.8
	48S	-6.8	-13.0	-9.4	-15.6	-11.2	-1.0	-8.1
	68S	-12.7	-13.2	-12.5	-16.3	-8.6	3.3	-6.0

TABLE 24. The vertically integrated northward transport of heat in the Atlantic as given by this study using 20^{o} ocean segments for the surface down to 1000 m and by Lamb and Bunker (1982) for the surface to 300 m and 500 m in units of 10^{15} W.

Present Study		Lamb and Bunker		
	Jan-Feb		Jan-Feb	
Latitude	1000m	Latitude	300m	500m
72 N	.1	70 N	.1	.1
52 N	.5	50 N	1.3	1.7
32 N	.9	30 N	1.0	1.2
12 N	.9	10 N	.8	1.2
8 S	.3	10 S	.3	.5
	May-June-July		May-June	
Latitude	1000m	Latitude	300m	500m
72 N	.1	70 N	.1	.1
52 N	-.5	50 N	.3	.4
32 N	-.7	30 N	1.3	1.6
12 N	-1.4	10 N	.5	.9
8 S	-1.2	10 S	-.5	0.0

and location northward heat transport ($F_0 > 0$) found using the 20^o ocean segments seems physically more realistic than southerly transport indicated by the 32^o segments. Additionally, the 20^o values are in qualitative agreement with the works of Oort and Vonder Haar (1976) and Lamb and Bunker (1982), both of which show large northward transports between 10^oN-50^oN. During the months of May, June and July the three studies give conflicting results. Oort and Vonder Haar obtained positive values of F_0 for May for the entire Northern Hemisphere while we found negative values south of 60^oN. The results of Lamb and Bunker indicate northward heat transport in the Atlantic for all latitudes north of the equator, in contrast with our results (Table 24). Both Oort and Vonder Haar, and Lamb and Bunker estimated the magnitude of the uncertainties and found them to be quite large, i.e. of the same order as F_0 itself, indicating the difficulting of accurately computing the meridional oceanic heat transport.

D. Errors and sensitivities

The feasibility of using the column budget method to determine the atmosphere-ocean energy balance depends on the errors and sensitivities of each of the budget components. In general, it is difficult to separate the many potential sources of uncertainty and their subsequent impact on the budget calculations. Deficiencies in the data and data assimilation procedure, the error, and the budget method itself all contribute to inaccuracy in the budget results.

1. Data and data assimilation errors

The many instruments used to obtain meteorological and oceanographic data are subject to both random and systematic errors. During the FGGE year several observing systems were employed to measure the atmosphere, each having different error characteristics and sampling distributions. The Japanese Meteorological Agency (1981) investigated this problem and found that inhomogeneities in the data density, satellite wind estimates from geostationary satellites, and the lag time between observations and their insertion into the model all significantly affect accuracy.

There are many uncertainties associated with assembling data and incorporating it into a GCM (McPherson, 1975; Bengtsson, 1985). Interpolation of the data to gridpoints combines and alters the various errors in an unknown manner. Data insertion causes imbalances between the mass and motion fields, and high frequency gravity wave noise. The model physics must also adjust (or spin-up) to the newly inserted data. Long spin-up times mean that each analysis causes a shock which affects the model forecast. This adjustment period appears to take from several days to over a week (Bengtsson, 1981; Schubert and Herman, 1981). Two outstanding problems in data assimilation are: the incorporation of moisture data into a model and the analyses of mass and motion fields in the tropics. In addition, the assimilation procedure may smooth out unwanted small scale variablity but at the same time reduce horizontal gradients, decreasing the divergence of energy transport.

The heat contained in a 1000 m column of ocean is on the order

of 10^{10} J m^{-2} while month-to-month changes in the heat content are less than 0.005 % of this value. Thus calculating the monthly change in heat storage involves taking the difference between very large numbers having similar values, making it difficult to obtain accurate results. Using data from the North Pacific, Wyrtki and Uhrich (1982) assessed the uncertainty of heat storage estimates by evaluating measurement and sampling errors and by comparing simultaneous observations. They found that both instrument error and environmental variablity on small time and space scales have a large impact on the computation of ocean heat storage. Due to the greater temperature difference between the surface and 100 m, the errors were larger in summer than in winter. Wyrtki and Uhrich estimated that the maximum error in monthly mean values of S_0 is on the order of 100 W m^{-2}. They concluded it was not feasible to compute S_0 on a monthly basis but that such estimates were possible over a complete heating or cooling season.

2. Model errors

Integrating the GLA GCM for six hours tends to suppress the spurious high frequency oscillations caused by the insertion of data but introduces errors inherent to numerical models. The errors caused by the finite difference representation of time and spatial derivatives are believed to be small, due to the short duration of the forecast. The relatively coarse horizontal and vertical resolution appear to be adequate in handling the general circulation

(Halem et al. 1978), but may misrepresent smaller features. The poor resolution in the boundary layer may significantly degrade the budget results (Swinbank, 1983).

Perhaps the most important source of model error is caused by the parameterization of diabatic processes, including radiation, cloud formation and precipitation, and the surface sensible and latent heat flux. Using satellite data, Oort and Vonder Haar (1976) have estimated the uncertainty in the net radiation at the top of the atmosphere to be 10 W m^{-2} for a 10^{o} latitude band. Ellis et al. (1978) have proposed that the uncertainty in the global mean net radiation is approximately 10 W m^{-2}, which implies larger errors for regional estimates of F_T. The net radiation values computed by the GLA model appear to be 25-40 W m^{-2} greater than those given by satellite observations. In Section 5A the error was linked to an overestimation of the absorption of shortwave radiation at the earth's surface. In addition, the simple parameterization of the formation, type and extent of cloud cover may significantly affect radiative and dynamic processes (Simpson, 1973).

3. Uncertainties in the budget method

Inaccuracies are also introduced by assumptions and procedures used in the column budget method. The uncertainty in the budget results is increased by: neglecting certain processes such as the storage of heat by land and ice, computing terms from the difference between large numbers, and the propagation of error through the budget equations. The energy balance components may also be

sensitive to the size, location and vertical dimension of the budget box. Several experiments are conducted to examine some of the sensitivities and errors in the column budget method.

a. Sensitivity to size and location of the budget box

Budget calculations are performed for five additional regions in the North Pacific (Fig. 6) to investigate how variations in the size and location of the budget box affect the energy balance results. Regions 35 through 37 are similarly located but become consecutively smaller, while regions 38 and 39 are narrower and centered further to the north. Table 25 gives the values of the various budget terms for these regions. Differences of 10-15 W m^{-2} in the value of div F_A are found between regions 35, 36, and 37 during both winter and summer, with similar differences between regions 38 and 39. Bretherton et al. (1982) estimated that small changes in the regional boundaries could alter div F_A values by as much as 25 W m^{-2}. The high degree of variablity in the atmospheric energy flux divergence (shown in Fig. 7) makes it highly sensitive to the placement of the budget column. As found by Oort (1983) and Burridge (1985), the field is dominated by dipole-like structures especially noticeable over the Himalayas and Greenland Plateau. These features are well correlated with systematic errors in the mass divergence field and may be associated with slow gravity modes caused by the insertion of data into the model. However, the full explanation for these biases and the best way to remove them requires further study.

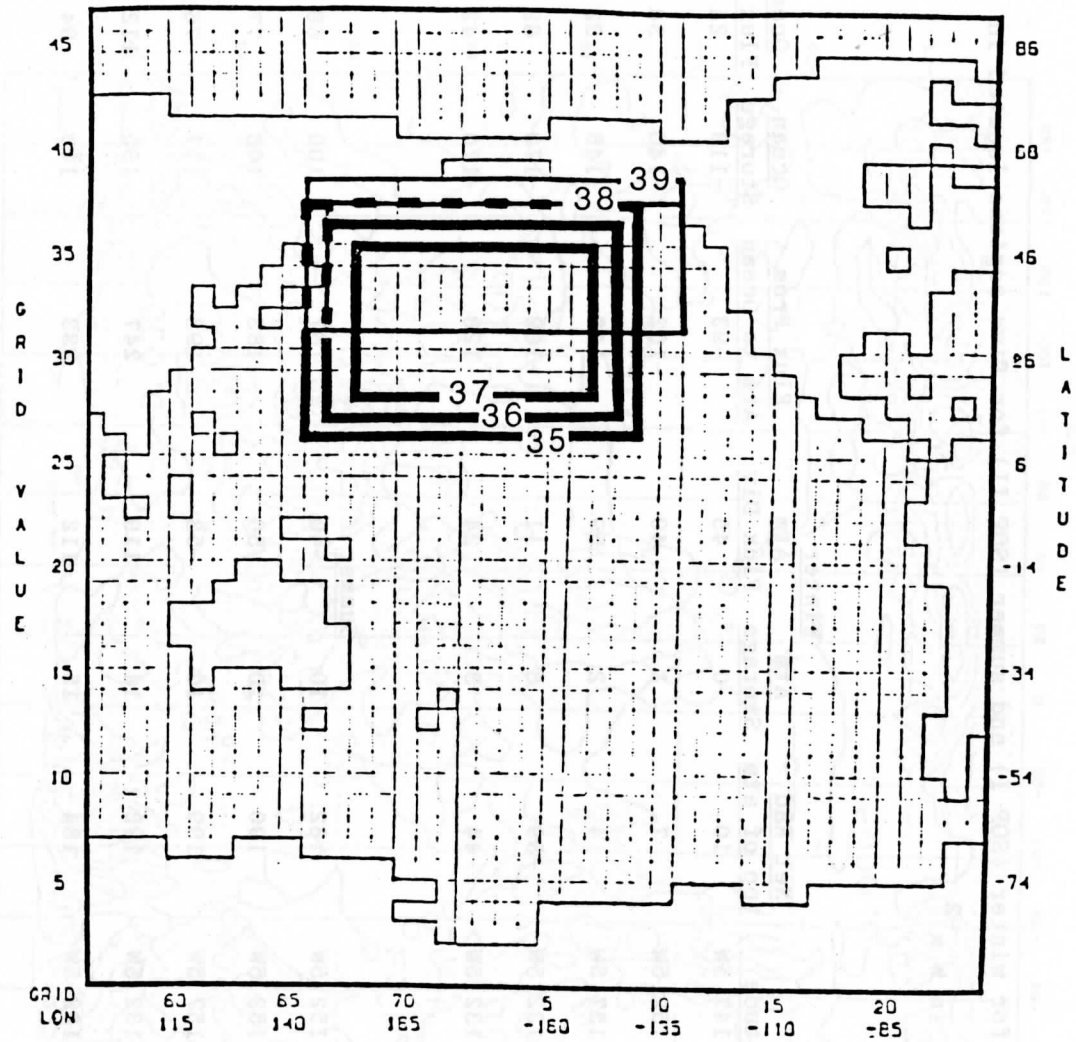

Fig. 6. Regions 35 through 39.

TABLE 25. The budget terms for winter (SOP I) and summer (SOP II) for five regions located in the North Pacific in W m^{-2}.

Region	Latitude	Longitude	Net Rad top of atm	Atm Storage	Atm Flux Div	Flux From Atm to Ocean	Ocean Storage	Ocean Flux Div
				Winter				
35	12N-56N	142.5E-147.5W	10	0	45	-93	-118	24
36	16N-52N	147.5E-152.5W	7	1	49	-102	-140	38
37	20N-48N	152.5E-157.5W	4	2	59	-116	-148	32
38	32N-56N	147.5E-132.5W	-39	3	11	-109	-170	62
39	32N-60N	142.5E-132.5W	-44	3	24	-128	-170	42
				Summer				
35	12N-56N	142.5E-152.5W	182	10	-40	167	100	68
36	16N-52N	147.5E-152.5W	190	10	-50	183	106	77
37	20N-48N	152.5E-157.5W	199	10	-53	193	117	76
38	32N-56N	147.5E-132.5W	192	14	-119	247	135	112
39	32N-60N	142.5E-132.5W	184	15	-112	233	140	94

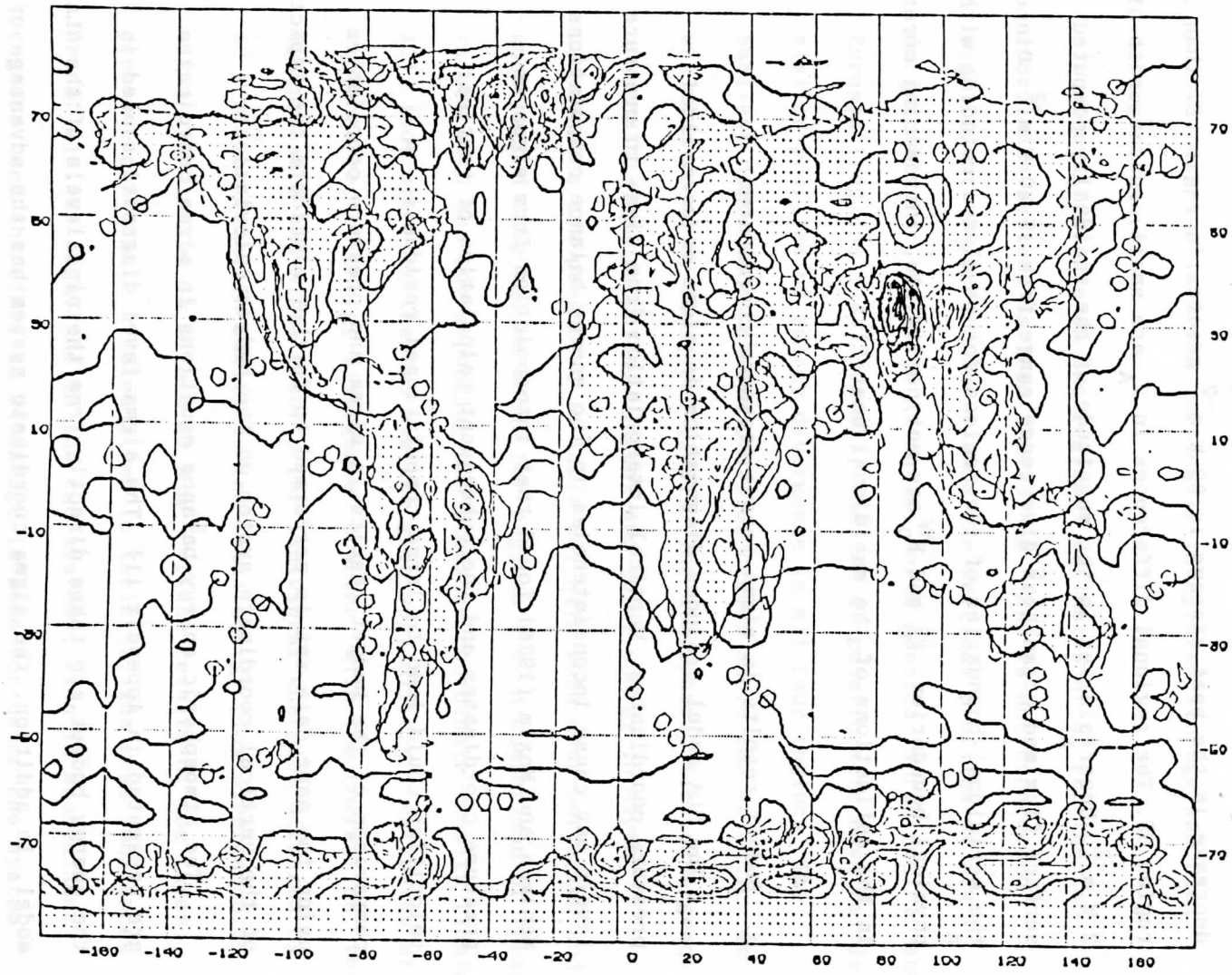

Fig. 7. The atmospheric flux divergence of total energy (W m^{-2}). Contour intervals are every 2000 W m^{-2}, with the dashed lines representing contours with negative values.

Significant differences between regions also occurred in the values obtained for F_T and especially S_0. During winter, the decrease in the heat storage is 30 W m^{-2} greater in region 37 than in region 35. The regional differences in S_A are small, on the order of 2 W m^{-2}. Uncertainties in the magnitude of the residually computed surface flux and ocean heat divergence range from 15-20 W m^{-2}. Since the meridional boundaries of the regions do not always coincide with physical boundaries, $\bar{F}_0^E$ and $\bar{F}_0^W$ are not negligible, introducing error in the estimations of the meridional heat flux.

b. Budget results in sigma versus pressure coordinates

The GLA model produces diagnostics in sigma or normalized pressure coordinates. Vertical interpolation from sigma to pressure levels may cause inconsistencies in the energy balance computations. Mahlman and Moxim (1976) found that interpolation from sigma to pressure coordinates and the subsequent calculation of vertical velocities could lead to large computational residuals . A comparison of the budget results in sigma and pressure coordinates using the same data set is performed to further elucidate the impact of the vertical coordinate system on the budget calculations.

The atmospheric energy balance equations in sigma coordinates are presented in Appendix III. The sigma level diagnostics used in the energy budget are taken directly from the nine levels of the GLA model. In addition, the sigma coordinate system has the advantage of a constant bottom boundary (σ=1) at the earth's surface. It should be noted that the limits of the pressure and sigma coordinate

systems are not identical. Thus, the extrapolation procedure (see Appendix III) used to match their upper and lower boundaries may introduce error into the vertically integrated storage and flux divergence terms.

The difference in the regional estimates of S_A for the two coordinate systems is less than 3 W m^{-2} and is not considered significant. Figures 8 and 9 show the vertical profiles of div F_A during July for the North Atlantic, North America, North Pacific and Eurasia (regions 1-4). Overall, the two diagnostic sets have fairly similar profiles of energy divergence in all four regions. The smallest difference between profiles occurs above the Atlantic, as was also found by Sävijarvi (1981). The atmospheric flux divergence of sensible, geopotential, latent and total energy in sigma coordinates are presented in Table 26, with both mass-corrected and uncorrected July values shown for regions 1-4. A comparison of these values with the corresponding GLA pressure coordinate results (Table 12), indicate that the two systems give very different estimates of the uncorrected energy divergence. However, with the correction, the GLA pressure and sigma results for individual energies differed by 25 W m^{-2} or less. In addition, the total energy flux divergence in sigma coordinates is within 20 W m^{-2} of the results of the three pressure coordinate studies given in Table 12. The mass imbalances are of similar magnitude in the two systems, even in mountainous regions, and therefore no advantage is seen for using one system over the other.

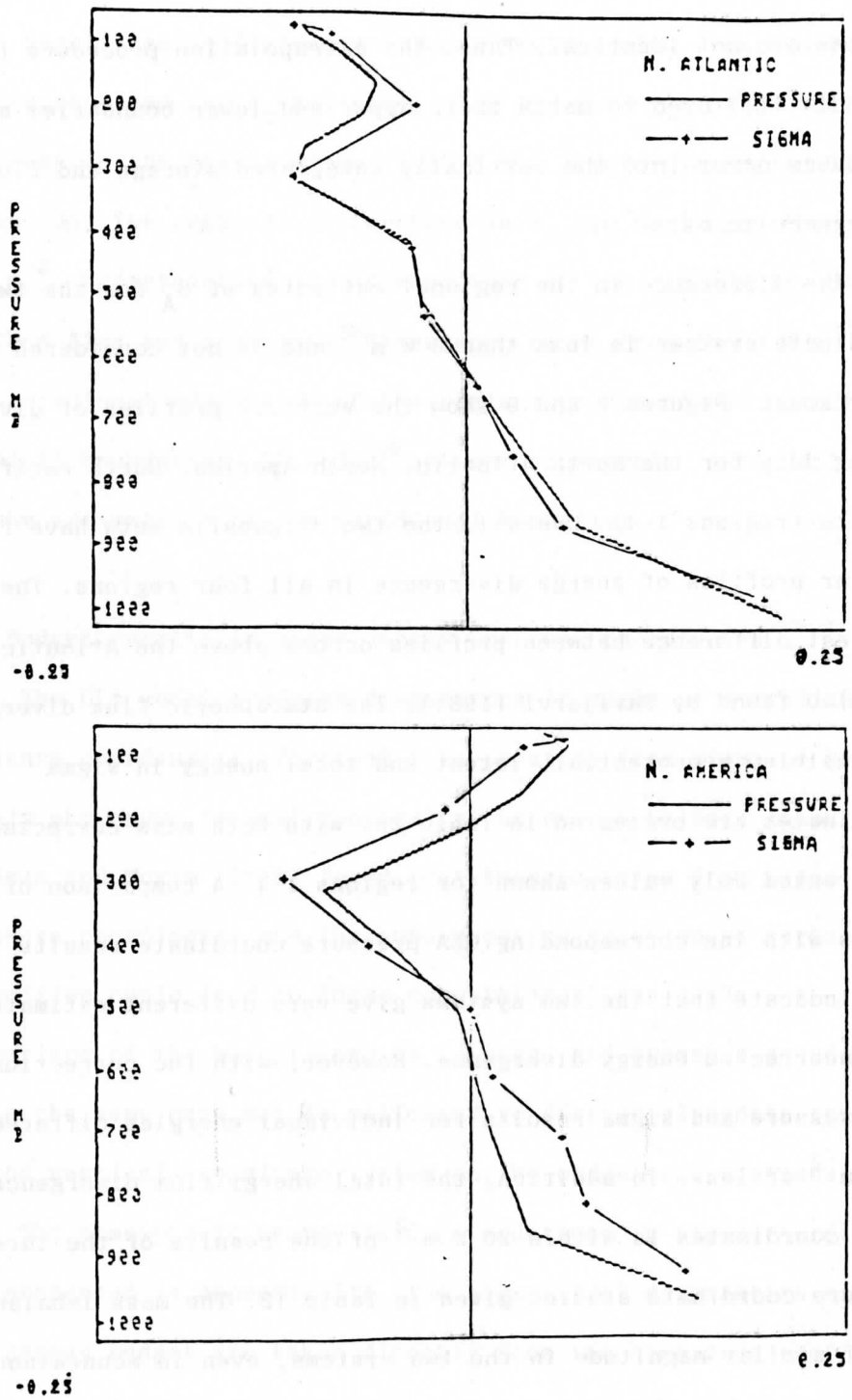

Fig. 8. The energy flux divergence profile (J Kg^{-1} sec^{-1}) for the North Atlantic and North American regions.

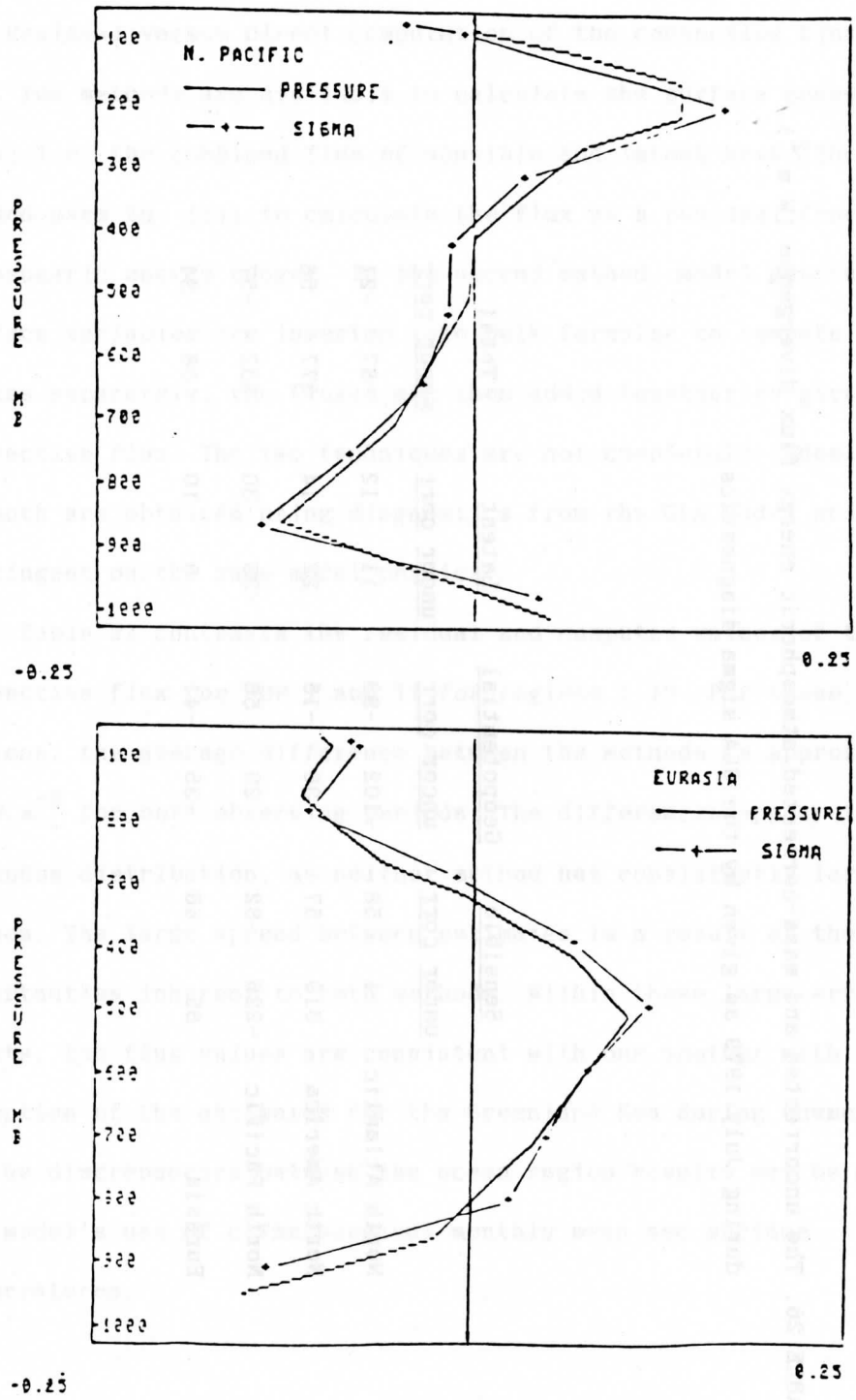

Fig 9. Same as Fig. 8 but for the North Pacific and Eurasian regions.

TABLE 26. The uncorrected and mass-corrected atmospheric energy flux divergence (W m^{-2}) during July 1979 as given by the GLA sigma diagnostics.

	Sensible		Geopotential		Latent		Total	
	uncor	corr	uncor	corr	uncor	corr	uncor	corr
North Atlantic	4	58	-102	-93	11	12	-87	-21
North America	319	57	36	-15	22	14	377	56
North Pacific	-226	-82	29	56	-35	-30	-232	-57
Eurasia	85	66	-35	-41	9	10	58	34

c. Residual versus direct computation of the convective flux

Two methods are available to calculate the surface convective flux, i.e. the combined flux of sensible and latent heat. The first method uses Eq. (14) to calculate the flux as a residual from the atmospheric energy budget. In the second method, model generated surface variables are inserted into bulk formulae to compute the two fluxes separately; the fluxes are then added together to give the convective flux. The two techniques are not completely independent as both are obtained using diagnostics from the GLA model and are contingent on the same model physics.

Table 27 contrasts the residual and computed values of the convective flux for SOP I and II for regions 1-19. For these regions, the average difference between the methods is approximately 30 W m^{-2} for both observing periods. The differences appear to have a random distribution, as neither method has consistently larger values. The large spread between estimates is a result of the many uncertanties inherent to both methods. Within these large error limits, the flux values are consistent with one another with the exception of the estimates for the Greenland Sea during summer. Some of the discrepancies between the ocean region results may be due to the model's use of climatological monthly mean sea surface temperatures.

d. Error propagation

Calculation of the atmospheric storage and energy flux divergence requires measurements of temperature, wind, geopotential

TABLE 27. The sum of the surface sensible and latent heat flux ($W\ m^{-2}$) during the two Special Observing Period as computed from the residual of the atmospheric energy budget (14), and directly by the GLA model.

		SOP I		SOP II	
Region	Location	Residual	Computed	Residual	Computed
1	N. Atlantic	200	181	87	66
2	N. America	43	62	150	125
3	N. Pacific	187	172	75	54
4	Eurasia	91	69	133	143
5	Europe	76	28	149	98
6	Caribbean	235	198	157	113
7	N. Africa	117	181	155	174
8	S. Africa	149	187	101	149
9	S. America	152	202	115	136
10	Australia	128	158	114	128
11	Antarctic O.	87	42	135	88
12	S. Atlantic	145	115	127	129
13	S. Pacific	143	121	163	145
14	Indian O.	156	126	147	167
15	C. Atlantic	182	146	152	95
16	C. Pacific	188	161	161	109
17	N. Atlantic	189	191	48	48
18	N. Pacific	154	153	22	20
19	Greenland Sea	105	124	-53	35

height and moisture. Questions arise as to how inaccuracies in each of these variables will impact the values obtained for S_A and div F_A. Random and systematic errors in these components will propagate through the budget calculations and affect the results obtained for the surface energy flux and the divergence of heat transport within the ocean.

An error analysis is performed by generating random errors and then adding them to the atmospheric variables each time the variables are extracted from the model. The errors are produced by first prescribing rms errors in the variables as a function of height (Table 28). The rms errors in wind and temperature are estimated by averaging the errors in various observing systems during FGGE, given by Bengtsson et al. (1982). The height errors were obtained from Lorenc et al. (1980). These errors include the uncertainties in instrument measurements and the effects of phenomena which are smaller than the scale that can be analyzed (eg. thunderstorms). The rms values are then multiplied by a number randomly generated from a pseudo-normal function (a normal distribution with a mean of zero and standard deviation of one but which is limited to within three standard deviations of the mean).

The values given by the error analysis are approximate, as the actual errors are functions of time and horizontal location in addition to height. Furthermore, the observations are assimilated by the GLA GCM and thus rms error in the diagnostics used in the budget calculations are different from those given in Table 28. These problems aside, the analysis provides estimates of the magnitude of

TABLE 28. RMS error estimates as a function of height. The wind and temperature values were derived by averaging errors of the different observing systems used by Bengtsson et al. (1982) and the height errors are taken from Lorenc et al. (1980).

Presure level (mb)	Wind (m/sec)	Temperature (^{o}C)	Height (m)
50	8.2	2.8	47.2
70	8.2	2.5	46.1
100	8.2	2.0	44.9
150	8.2	1.9	41.4
200	8.2	1.9	37.8
250	8.2	1.9	32.9
300	8.2	1.8	29.1
400	7.2	1.8	24.0
500	6.7	1.8	21.0
700	5.5	1.7	14.4
850	4.7	1.8	10.6
surface	4.7	2.3	6.6

(Due to a lack of information, the rms error in the specific humidity is obtained by assuming the rms error in the dew point temperature is the same as the rms error in the temperature.)

the errors in the atmospheric budget calculations.

The impact of random errors on div F_A and S_A is determined by taking the difference between the analysis with random errors added and the original (baseline) analysis. The averaging procedures used to obtain the divergence and storage values give mean estimates of the effects of random errors, and are therefore similar to Monte Carlo methods.

The magnitude of the difference between the error and baseline estimates of the individual and total energy flux divergences for January are shown in Table 29. The errors greatly alter the uncorrected flux divergence of sensible heat and the total energy divergence. For the 19 regions shown, this difference has an average value of 30 W m^{-2}, and exceeds 50 W m^{-2} in several regions. Surprisingly, the random errors are almost entirely compensated for by the mass balance correction. After the correction is applied the error and baseline estimates of div F_A differ by an average of 3 W m^{-2}. Hastenrath (1980) estimated that random error in the net atmospheric export of energy was 5 W m^{-2} in a belt extending from 0^{o}-30^{o}N. The changes in S_A due to random errors are also small, on the order of 1-2 W m^{-2}.

When a systematic error is introduced into all wind vectors, i.e. the wind speed is increased by 10% at every grid point, the error propagates through the budget calculations causing a similar bias in the value of div F_A (not shown). Horizontally varying systematic errors may have a more complex and severe impact on the budget computations. The largest errors in div F_A are likely due to

TABLE 29. The magnitude of the difference between the original energy flux divergence and the energy flux divergence with the random errors added (W m^{-2}). Results are for both uncorrected and mass-corrected energy divergences during January.

		Sensible		Potential		Latent		Total	
Region	Location	uncor	cor	uncor	cor	uncor	cor	uncor	cor
1	N. Atlantic	40	2	6	3	0	0	46	2
2	N. America	16	0	1	4	1	1	17	1
3	N. Pacific	20	1	7	2	0	0	27	1
4	Eurasia	1	0	1	1	0	0	0	2
5	Europe	51	4	32	18	1	0	83	14
6	Caribbean	33	0	6	2	3	2	43	0
7	N. Africa	27	4	2	7	1	1	28	2
8	S. Africa	50	3	17	3	1	2	66	3
9	S. America	14	0	2	2	1	1	16	3
10	Australia	104	2	30	3	1	3	135	2
11	Antarctic O.	5	2	4	2	1	1	8	0
12	S. Atlantic	6	4	8	6	2	2	16	1
13	S. Pacific	14	1	5	1	2	1	21	2
14	Indian O.	46	1	8	3	2	1	58	1
15	C. Atlantic	42	0	7	3	0	0	49	4
16	C. Pacific	22	3	0	5	1	1	24	1
17	N. Atlantic	23	2	4	9	0	1	17	9
18	N. Pacific	15	3	1	4	1	1	16	1
19	Greenland Sea	33	4	28	19	1	1	63	16

systematic errors in the wind field (Lorenc and Swinbank, 1984); we will focus on one well documented bias in wind speed estimates.

Kållberg et al. (1982) found that during the FGGE year satellite cloud track motions generally underestimated the wind speed, especially in regions containing strong winds, as in the midlatitude and subtropical jet streams. They proposed two possible explanations for this negative bias: the assigned cloud height may be incorrect and the cirrus cloud motions may be slower than the flow. Satellite observations are the primary source of wind data over the oceans and ice sheets but play a much less significant role over land. For example, satellite winds are not assimilated over N. America in the GLA analysis (Halem et al. 1982). The distribution and magnitude of the resulting systematic error caused by incorporating these winds into the analysis are greatly modified by the model's assimilation procedure. To approximate this bias, wind speeds are reduced by 10% over oceans and ice but are not changed over land.

The biased energy divergence minus the original divergence gives the systematic error impact which is shown for January in Table 30. The wind biases cause very large errors in the uncorrected sensible and geopotential energy divergences. These errors are on the order of several hundred W m^{-2} and exceed 400 W m^{-2} over Europe. As expected, the greatest energy divergence errors are correlated with the maximum error in the wind bias, i.e. the location of the winter time jet streams.

The mass balance correction significantly reduced but did not

TABLE 30. The difference between the original energy flux divergence subtracted from the energy flux divergence with the systematic errors added (W m^{-2}). Results are for both uncorrected and mass-corrected energy divergences during January.

Region	Location	Sensible		Potential		Latent		Total	
		uncor	cor	uncor	cor	uncor	cor	uncor	cor
1	N. Atlantic	111	-9	42	13	0	-2	155	2
2	N. America	-119	10	-59	-25	1	-1	179	-16
3	N. Pacific	272	-27	116	43	0	-6	391	13
4	Eurasia	-228	8	-80	-17	-1	2	-311	-9
5	Europe	417	-19	163	53	4	0	587	36
6	Caribbean	106	-28	78	44	-5	-8	178	8
7	N. Africa	0	0	0	0	0	0	0	0
8	S. Africa	-12	-1	-3	0	-1	0	-15	0
9	S. America	-213	5	-64	-8	-5	3	-283	1
10	Australia	23	11	-25	-16	2	4	5	-2
11	Antarctic O.	-13	3	-9	-5	1	1	-21	-1
12	S. Atlantic	30	-8	20	11	-2	-4	48	-1
13	S. Pacific	68	0	17	0	2	-1	87	-1
14	Indian O.	16	-3	8	3	0	-1	25	0
15	C. Atlantic	-13	5	-12	-7	1	2	-24	-1
16	C. Pacific	19	-2	8	3	-1	-1	29	0
17	N. Atlantic	35	-8	21	10	-1	-2	55	1
18	N. Pacific	358	-23	137	44	1	-4	501	21
19	Greenland Sea	143	-5	64	26	1	1	210	23

eliminate the errors. Correcting for mass imbalances caused by both random and systematic error is crucial for obtaining reasonable results for div F_A. The corrected error and baseline estimates of sensible and geopotential energy divergence differed by as much as 50 W m^{-2}. The error impact on the kinetic (not shown) and latent energies is much smaller, generally less than 2 and 5 W m^{-2}, respectively. In many regions the errors in the geopotential and sensible flux divergence were of opposite sign and partially cancelled when summed with the kinetic and latent energies to give the total energy divergence. The errors in div F_A, though less than the errors in the individual energies, can exceed 20 W m^{-2} for regions containing strong winds. This indicates that systematic errors may have a significant impact on the atmospheric energy divergence and on the energy balance calculations as a whole.

VI Summary and Conclusion

The winter and summer energy balance of the earth-atmosphere system were examined for selected regions distributed around the globe. The column budget technique employed by Oort and Vonder Haar (1976) was used to obtain estimates of the atmospheric and terrestrial energy balance. These estimates were employed to determine the accuracy and physical consistency of the budget components and to assess the feasibility of using the column budget method to estimate the meridional ocean heat transport.

In the atmosphere, the net radiation at the top of the column was combined with estimates of the time change in energy storage and flux divergence of energy to obtain the flux through the surface as a residual. This surface flux became the input to the top of the terrestrial budget, and the energy it provided was either stored by the ocean or exported via ocean currents, as the energy stored by land and ice was considered negligible. The net radiation at the top of the atmosphere was generated by the GLA model physics. The GLA level IIIb analysis from the SOPs of the FGGE was used to compute the storage and divergence of energy in the atmosphere. A long term record of NODC oceanographic temperature observations was employed to calculate the ocean heat storage. The flux divergence of energy in the ocean was obtained as a residual from the difference between the surface energy flux and the time rate of change of the ocean heat storage.

Analyses of the budget components provided information about the

seasonal circulation of the atmosphere and ocean. A surplus of net radiation at the top of the atmosphere was found for regions located between 35^{o}N-35^{o}S. Both the oceans and the atmosphere exported significant amounts of energy from the tropics to midlatitudes. During winter between 30^{o}-60^{o} in both hemispheres, a large quantity of energy (> 200 W m^{-2}) was transferred from the ocean to the atmosphere via fluxes of sensible and latent heat. This energy was supplied by poleward currents and the energy stored in the oceans during the summer. The atmosphere transported the energy to the continental and polar heat sinks. In the summer months, energy imparted from the warm continents to the overlying air was exported to the cooler oceanic regions. This seasonal exchange of energy between the continents and oceans was found to be much stronger in the Northern Hemisphere than in the Southern Hemisphere due to the limited land mass and therefore smaller air-sea contrasts in the Southern Hemisphere.

The flux divergence of energy in the atmosphere was partitioned into four constituents: kinetic, sensible, geopotential and latent energies. The sensible and geopotential energies were greater in magnitude but tended to balance one another. The flux divergence of latent energy also played a significant role in the atmospheric energy balance. A correction applied to conserve mass in the atmospheric column proved essential to obtaining reasonable energy flux divergence estimates. After the correction was incorporated, the energy flux divergence estimates differed by 15-30 W m^{-2} from the results of Swinbank (1983), Bretherton et al. (1982) and Alestalo

(1981) for various regions in the Northern Hemisphere.

The potential sources of uncertainty in the data, GLA model and the column budget method were discussed. Data deficiencies, instrument bias in multiple observing systems, and subgrid-scale processes may have a significant impact on the accuracy of the atmospheric flux divergence of energy and the ocean heat storage. Difficulties faced in using a GCM assimilation system include spurious gravity oscillations and spin-up error caused by data insertion, and inaccurate representation of diabatic processes. Progress towards reducing these errors is closely associated with improvements in data assimilation methods and model physics.

Several experiments were performed to investigate some of the uncertainties in the column budget method, the results of which indicated:

1) Small displacements in the regional boundaries affected all budget components and were shown to alter the flux divergence of energy in the atmosphere and the time tendency of ocean heat storage by as much as 20-30 W m^{-2}.

2) Differences between the atmospheric energy flux divergence computed in sigma and pressure coordinates were found to be less than 20 W m^{-2}. The mass imbalances were of similar magnitude when calculated using the two coordinate systems and thus no advantage is seen for using one system in place of the other.

3) The combined flux of sensible and latent heat across the earth-atmosphere interface was computed as a residual from the

atmospheric budget and directly, by employing bulk aerodynamic formulae. On average, the two techniques differed by 30 W m^{-2} during both winter and summer. These differences appear to be randomly distributed.

4) Random errors introduced into the atmospheric variables were compensated for by the mass balance correction, causing a negligible impact (<5 W m^{-2}) on the atmospheric flux divergence of energy. A 10% decrease in the wind speed over the oceans was shown to have a significant effect on the flux divergence of energy in the atmosphere. The wind biases altered the budget results by more than 20 W m^{-2} for regions in proximity to the polar and subtropical jets.

The oceanic meridional heat flux was obtained using Green's theorem by integrating the heat flux divergence over zonal segments extending the width of the ocean basin. The ocean heat transport was found to be very sensitive to systematic errors, as the integration procedure used to compute heat transport compounds inaccuracies in all the budget terms. The model generated shortwave radiation absorbed at the earth's surface was found to have a positive bias of approximately 25-40 Wm^{-2} with the greatest error occurring during the summer months. This error propagated through the budget calculations causing excessive southward heat transport estimates in the Southern Hemisphere in January and February and at all latitudes during the Northern Hemisphere summer (Oort and Vonder Haar, 1976; Lamb and Bunker, 1982).

In the column budget method, the monthly mean ocean heat flux divergence is calculated from the difference between the surface

energy flux and the rate of change of ocean heat storage. Through sensitivity experiments and comparisons with other studies, the uncertainty in the net surface flux is estimated to be on the order of 30 Wm^{-2}, in agreement with the error evaluation of Hastenrath (1980). The monthly change in heat storage is poorly known, with errors possibly as large as 100 Wm^{-2} (Wyrtki and Uhrich, 1982). Burridge et al. (1982) indicated that an error of 10 W m^{-2} or less in the ocean heat flux divergence was necessary to calculate the meridional ocean heat transport to within a desired accuracy of 20%. Presently, it is not possible to obtain this level of accuracy using the column budget method. This conclusion was also reached by Holopainen and Fortelius (1986), and Boer (1986).

Several tests exist for verifying the accuracy of the energy budget components. These include:

1) Over land, the net radiation at the top of the atmosphere should be equal to the atmospheric energy flux divergence in the annual average.

2) Successive integration of the flux divergence of energy in the ocean in the meridional direction would require the ocean heat transport to be zero at both the northern and southern boundaries. In the present study, this condition was violated as large southward fluxes of heat were found near the Antarctic coast. These fluxes were linked to excessive absorption of solar radiation at the surface.

3) Detailed statistics generated by GCMs can be compared to

observations and budget output. For example, several radiosonde stations were shown to have large biases in their observations when compared to the ECMWF first guess fields (Hollingsworth et al. 1985b).

Applying these methods to locate and remove systematic errors may significantly improve the accuracy of the energy balance computations.

Bibliography

Aagard, K., and P. Greisman, 1975: Toward new mass and heat budgets for the Arctic Ocean. J. Geophys. Res., 80, 3821-3827.

Alestalo, M., 1981: The energy budget of the earth-atmosphere system in Europe. Tellus, 33, 360-371.

Apruzese, J.P., M.R. Schoeberl, and D.F. Strobel, 1982: Parameterization of IR cooling in a middle atmosphere dynamics model. 1. Effects on the zonally averaged circulation. J. Geopys. Res., 87, 8951-8966.

Arakawa, A., 1972: Design of the the UCLA atmospheric general circulation model. Tech rept. No. 7, Dept. of Meteorology, University of California at Los Angeles.

Baker, W.E., 1983: Objective analysis and assimilation of observational data from FGGE. Mon. Wea. Rev., 111, 328-342.

Bengtsson L., 1981: Data analysis, initialization, and data assimilation. International Conference of Preliminary FGGE Data Analysis and Results, Bergen, Norway, 23-27 June, 1980. WMO, Geneva, pp. 162-185.

___, 1985: Four dimensional data assimilation. Seminar/Workshop on Data Assimilation Systems and Observing System Experiments With Particular Emphasis on FGGE. Vol. 2, 3-11 September, 1984. ECMWF, Reading, U.K., pp. 1-6.

___, M. Kanamitsu, P. Kallberg and S. Uppala, 1982: FGGE 4-dimensional data assimilation at ECMWF. Bull. Amer. Meteor. Soc., 63, 43.

Boer, G.J., 1986: A comparison of mass and energy budgets from two FGGE data sets and a GCM. Mon. Wea. Rev., 114, 885-902.

Bretherton, F.P., D.M. Burridge, J. Crease, F.W. Dobson, E.B. Krause, and T.H. Vonder Haar, 1982: The cage experiment a feasibility study. WMO, World Climate Program Office, Geneva.

Bryan, K., 1962: Measurements of meridional heat transport by ocean currents. J. Geophys. Res., 67, 3403-3414.

___, 1969: A numerical method for the study of the circulation of the world ocean. J. Comput. Phys., 4, 347-376.

___, and L.J. Lewis, 1979: A water mass model of the world ocean. J. Geophys. Res., 34, 2503-2517.

___, S. Manabe, and R.L. Pacanowski, 1975: A global-ocean-atmosphere climate model. Part II. The ocean circulation. J. Phys. Oceanogr., 5, 30-46.

Bryden, H.L. and M.H. Hall, 1980. Heat transport by currents across 25°N in the Atlantic Ocean. Science, 207, 884-886.

Budyko, M.L., 1963: Atlas of the heat balance of the earth. (In Russian.) Moscow, Globnaia Geofiz. Obser., 69pp.

Burridge, D.M., 1985: Energy flux divergence calculations from ECMWF analyses for the FGGE year. WMO Global Weather Experiment Scientific Seminar, Helsinki. Garp Special Report No. 42, Geneva. pp. II 1-14.

Carissimo, B.C., A.H. Oort, and T.H. Vonder Haar, 1985: Estimating the meridional energy transport in the atmosphere and oceans. J. Phys. Oceanogr., 15, 82-91.

Cressman, G.P., 1959: An operational objective analysis system. Mon. Wea. Rev., 87, 367-374.

Ellis, J.S., T.H. Vonder Haar, S. Levitus, and A.H. Oort, 1978: The annual variation of the global heat balance of the earth. J. Geophys. Res., 83, 1958-1963.

Esbensen, S.K., and Y. Kushnir, 1981: The heat budget of the global ocean: an atlas based on estimates from surface marine observations. Report No. 29, Climatic Research Institute, Oregon State University, Corvalis, 219 pp.

Freeman, K.P. and K.N. Liou, 1979. Climatic effects of cirrus clouds. Adv. Geophys., 21, 231-287.

Fu, L-l, 1981: The general circulation and heat transport of the subtropical Atlantic as determined by the inverse method. J. Phys. Ocean., 11, 1171-1193.

Gabites, J.F., 1950: Seasonal variations in the atmospheric heat balance. Sc.D. thesis, Massachusetts Institute of Technology.

Gill, A.E., 1982: Atmosphere-Ocean Dynamics. Academic Press, New York, 662 pp.

Gruber, A., 1970: The energy budget over the Florida Penisula when a convective regime dominates. J. Appl. Meteor., 9, 401-416.

Halem, M., J. Shukla, Y. Mintz, M.L. Wu, R. Godbole, G. Herman, and Y. Sud, 1978: Comparisons of observed seasonal climate features with a winter and summer numerical simulation produced with the GLAS general circulation model. Proceedings of the JOC Study Conference on Climate Models, April 3-7, 1978, Washington D.C.

___, E. Kalnay, W.E. Baker, and R. Atlas, 1982: An assessment of the of the FGGE satellite observing system during SOP-1. Bull. Amer. Meter. Soc., 63, 407-426.

Hastenrath, S.L., 1966: On general circulation and energy budget in the area of the Central American Seas. J. Atmos. Sci., 23, 694-711.

___, 1980: Heat budget of tropical ocean and atmosphere. J. Phys. Oceanogr., 10, 159-170.

___, 1982: On the meridional heat transport in the world ocean. J. Phys. Oceanogr., 12, 922-927.

Holland, W.D. and A. Hirschman, 1972: A numerical calculation of the circulation in the North Atlantic Ocean. J. Phys. Oceanogr., 2, 336-354.

Hollingworth, A., A.C., Lorenc, M.S. Tracton, K. Arpe, G. Kats, S. Uppala, and P. Kallberg, 1985a: The response of numerical prediction systems to FGGE level IIb data. Part 1: Analyses. Quart. J. R. Met. Soc., 111, 1-66.

___, D.B. Shaw, P. Lonnberg, L. Illari, K. Arpe, and A.J. Simmons, 1985b: Monitoring of observation and analysis quality by a data assimilation system. Seminar/Workshop on Data Assimilation Systems and Observing System Experiments With Particular Emphasis on FGGE. Vol. 2, 3-11 September, 1984. ECMWF, Reading, U.K., pp. 293-347.

Holopanien, E.O. and C. Fortelius, 1986: On the accuracy of estimates of atmospheric large scale energy flux divergence. Mon. Wea. Rev. (accepted for publication).

Hsuing, J., 1985: Estimates of global oceanic meridional heat transport. J. Phys. Oceanogr., 15, 1405-1413.

Janowiak, J.E., A.F. Krueger, and P.A. Arkin, 1985: Atlas of Outgoing Longwave Radiation Derived from NOAA Satellite Data. NOAA Atlas No. 6, U. S. Government Printing Office, Washington, D.C., 44 pp.

Japanese Meteorological Agency, 1981: Results of an impact study on analysis and prediction of various combinations of the observing systems. International Conference of Preliminary FGGE Data Analysis and Results, Bergen, Norway, 23-27 June, 1980. WMO, Geneva, pp. 88-104.

Jung, G.H., 1952: Note on the meridional transport of energy by the oceans. J. Marine Res., 11, 139-146.

Kållberg P., S. Uppala, N. Gustafsson, and J. Pailleux, 1982: The impact of cloud tracked wind data on global analyses and medium range forecasts. ECMWF Tech. Rept. 34, Reading, England. 60 pp.

Kalnay, E., R. Balgovind, W. Chao, D. Edelmann, J. Pfaendtner, L. Takacs, and K. Takano, 1983: Documentation of the GLAS fourth order general circulation model. NASA Tech. Memo. 86064, NASA/ Goddard Space Flight Center, Greenbelt, MD.

Kung, E.C., 1967: Diurnal and long-term variations of the kinetic energy generation and dissipation for a five year period. Mon. Wea. Rev., 95, 593-606.

Lacis, A.A. and J.E. Hansen, 1974: A parameterization for the absorbtion of solar radiation in the earth's atmosphere. J. Atmos. Sci., 31, 118-133.

Lamb, P.J., and A.F. Bunker, 1982: The annual march of the heat budget of the North and tropical Atlantic. J. Phys. Oceanogr., 12, 1388-1409.

Lau, N-C. and A.H. Oort, 1981: A comparative study of observed Northern Hemisphere circulation statistics based on GFDL and NMC analyses. Part 1: the time mean fields. Mon. Wea. Rev., 109, 1380-1403.

Levitus S., 1982: Climatological Atlas of the World Ocean. NOAA Prof. Paper No. 13, U. S. Government Printing Office, Washington, D.C., 173 pp.

___, 1984: Annual cycle of temperature and heat storage in the world ocean. J. Phys. Oceanogr., 14, 727-746.

London, J., 1957: A study of the atmospheric heat balance. Final contract report, Contract AF19(122)-165, Dept. of Meteor. Oceanogr., New York University, 90pp.

Lorenc, A., I. Rutherford, and G. Larson, 1977: The ECMWF Analysis and data-assimilation scheme: analysis of mass and wind fields. ECMWF Technical Report No. 6, Reading, England, 46 pp.

___ and R. Swinbank, 1984: On the accuracy of general circulation statistics calculated from FGGE data - a comparison of results from two sets of analyses. Quart. J. R. Met. Soc., 110, 915-942.

Lorenz, E.N., 1967. The Nature and Theory of the General Circulation of the Atmosphere. World Meteorological Organization, Geneva, 161 pp.

Lyne, W.H., R. Swinbank, and N.T. Birch, 1982: A data assimilation experiment and the global circulation during the FGGE special observing periods. Quart. J. R. Met. Soc., 108, 575-594.

Mahlman, J.D., and W.J. Moxim, 1976: A method for calculating more accurate budget analyses of 'sigma' coordinate model results. Mon. Wea. Rev., 104, 1102-1106.

McPherson, R.D., 1975. Progress, problems and prospects in meteorological data assimilation. Bull. Amer. Met. Soc., 56, 1154-1166.

Newell, R.E., J.W. Kidson, D.G. Vincent, and G.J. Boer, 1974: The general circulation of the tropical atmosphere and interactions with the extratropical latitudes, Vol. 2. The MIT Press, Cambridge Mass., 371 pp.

O'Brien, J., 1970: Alternate solutions to the classical vertical velocity problem. J. Appl. Meteorol., 9, 197-203.

Oort, A.H., 1978: Adequacy of the rawinsonde network for global circulation studies tested through numerical model output. Mon. Wea. Rev., 106, 174-195.

___, 1983: Global Atmospheric Circulation Statistics, 1958-1973. NOAA Professional Paper 14, U. S. Government Printing Office, Washington, D.C., 180 pp.

___ and T.H. Vonder Haar, 1976: On the observed annual cycle in the ocean-atmosphere heat balance over the Northern Hemisphere. J. Phys. Oceanogr., 6, 781-800.

Palmen, E. and C.W. Newton, 1969: Atmospheric circulation systems. Academic Press, New York. 603 pp.

Pollard, D. and W.L. Gates, 1982: Diagnosis of the oceanic heat transport implied in an atmospheric GCM simulation. Report No. 29, Climatic Research Institute, Oregon State University, Corvalis, 20 pp.

Ramanathan, V. and R.D. Cess, 1974: Radiative transfer within the mesospheres of Venus and Mars. Astrophys. J., 188, 407-416.

Roemmich, D., 1980: Estimation of the meridional in the North Atlantic by inverse method. J. Phys. Ocean., 10, 1972-1983.

Sävijarvi, H., 1981: The energy budgets in North America, North Atlantic and Europe Based on ECMWF analyses and forecasts. ECMWF Tech. Rept. 27., Reading, U.K., 33 pp.

___, 1982: The mass balance in diagnostic studies: an example of analysed and forecast data calculations. Tellus, 34, 540-544.

Schubert, S.D. and Herman G.F., 1981: Heat balance derived from four-dimensional assimilations with a global circulation model. J. Atmos. Sci., 38, 1891-1905.

Sellers, W.D., 1965: Physical Climatology. The University of Chicago Press, 272 pp.

Shapiro, R., 1970: Smoothing, filtering and boundary effects. Rev. Geophys. and Space Phys., 8, 359-387.

Simpson, J., 1973: The Global Energy Budget and the Role of Cumulus Clouds. NOAA Tech. Memo. ERL WMPO-8, Boulder, Colorado, 175 pp.

Stephens, G.L., G.G. Campbell, and T.H. Vonder Haar, 1981: Earth radiation budgets. J. Geophys. Res., 86, 9739-9760.

Strobel, D.F., 1978: Parameterization of the atmospheric heating rate from 15 to 120 km due to O2 and O3 absorbtion of solar radiation. J. Geophys. Res., 83, 6225-6230.

Sud, Y.C., and J.A. Abeles, 1981: Calculation of surface temperature and surface fluxes in the GLAS GCM. NASA Tech. Memo. 82167, NASA/Goddard Space Flight Center, Greenbelt, MD., 24 pp.

Swinbank, R., 1983: A comparison of energy budget calculations based on ECMWF and Meteorological Office FGGE analysis. Met. O. 20 Technical Note II/213, Bracknell, U.K.

Vonder Haar, T.H. and A.H. Oort, 1973: New estimate of annual poleward energy transport by Northern Hemisphere Oceans. J. Phys. Oceanogr., 2, 169-172.

Vowinkel, E., and S. Orvig, 1970: The climate of the north polar basin. Climates of the Polar Regions, World Survey of Climatology, Vol. 14, chap 3., Elsevier, New York, 1970, pp. 129-252.

White, R.M., and B. Saltzman, 1956: On conversions between potential and kinetic energy in the atmosphere. Tellus, 8, 357-363.

Wu, M.L.-C, 1980: The exchange of infrared radiative energy in the troposphere. J. Geophys. Res., 85, 4084-4090.

Wunsch, C. 1978: The general circulation of the North Atlantic west of 50^{o} determined from inverse methods. Rev. Geophys. Space Phys., 16, 538-620.

Wyrtki K., and L. Uhrich, 1982: On the accuracy of heat storage computations. J. Phys. Oceanogr., 12, 1411-1416.

Appendix I

Development of The Atmospheric Energy Budget Equation

The kinetic energy equation in pressure coordinates can be written as

$$\frac{\partial K}{\partial t} + \vec{V}\cdot\nabla K + \frac{\partial K\omega}{\partial p} = -\vec{V}\cdot\nabla gz + \vec{V}\cdot\vec{F} \qquad (1)$$

where $\vec{V}\cdot\vec{F}$ is the frictional dissipation and ω the vertical velocity in pressure coordinates. The continuity equation in pressure coordinates,

$$\frac{\partial \omega}{\partial p} = -\nabla\cdot\vec{V} \qquad (2)$$

and the hydrostatic equation,

$$-\frac{1}{\rho} = \frac{\partial (gz)}{\partial p} \qquad (3)$$

can be combined with (1) and rearranged to give

$$\frac{\partial K}{\partial t} + \nabla\cdot(K + gz)\vec{V} + \frac{\partial (K + gz)\omega}{\partial p} = -\omega\alpha + \vec{V}\cdot\vec{F} \qquad (4)$$

where α is the specific volume.

The first law of thermodynamics can be expressed as

$$c_p \frac{\partial T}{\partial t} - \alpha \frac{\partial p}{\partial t} = S \tag{5}$$

where S is the diabatic heating rate. Using $\omega = dp/dt$ and then combining (5) with the continuity equation yields

$$c_p \frac{\partial T}{\partial t} + \nabla \cdot c_p T\vec{V} + \frac{\partial c_p T\omega}{\partial p} = S + \omega\alpha \tag{6}$$

Equating (4) and (6) and rearranging gives

$$\frac{\partial}{\partial t}(K + c_p T) + \nabla\cdot(K + c_p T + gz)\vec{V} + \frac{\partial}{\partial p}(K + c_p T + gz)\omega = \vec{V}\cdot\vec{F} + S \tag{7}$$

Vertically integrating (7), with constant limits of integration yields

$$\frac{\partial}{\partial t}\int_{P_T}^{P_S} (K + c_p T)\, dp/g + \int_{P_T}^{P_S} \nabla\cdot(K + c_p T + gz)\vec{V}\, dp/g = Q \tag{8}$$

where Q is equivalent to the sources and sinks of heat in the atmosphere which includes the fricitional dissipation, Q_{DIS}, net radiation, Q_{RAD}, sensible heat, Q_{SEN}, and latent heat, Q_{LAT}; i.e.,

$$Q = Q_{DIS} + Q_{RAD} + Q_{SEN} + Q_{LAT} \tag{9}$$

Q_{DIS} ($\int_{P_T}^{P_S} \vec{V}\cdot\vec{F}\, dp/g$) is neglected as regional estimates have shown it to be less than 5 W m^{-2} (Kung, 1967; Savijarvi, 1983). The net

radiation is equal to

$$Q_{RAD} = SW_A + LW_S - LW_T \tag{10}$$

the absorbed shortwave radiation plus the upward flux of longwave radiation from the surface minus the outgoing longwave radiation at the top of the atmosphere. The sensible heat sources result from fluxes through the surface,

$$Q_{SEN} = SH \tag{11}$$

If we neglect the flux of liquid water and ice through the sides of the column, the latent heat release is given by

$$Q_{LAT} \simeq LP \tag{12}$$

where P is the precipitation and L, the latent heat of condensation.

The water balance equation for an atmospheric column is

$$\frac{\partial}{\partial t} \int_{P_T}^{P_S} q \, dp/g + \int_{P_T}^{P_S} \nabla \cdot q\vec{V} \, dp/g = \sum \simeq E - P \tag{13}$$

where $\sum$, the net sources and sinks of water vapor, is approximately equal to the evaporation, E, minus precipitation. Multiplying (13) by L and then combining it with (12) gives

$$Q_{LAT} = -\frac{\partial}{\partial t}\int_{P_T}^{P_S} Lq\ dp/g - \int_{P_T}^{P_S} \nabla \cdot Lq\vec{V}\ dp/g + LH \qquad (14)$$

where LH is the latent heat flux at the surface ($L \cdot E$). Substituting (10), (11) and (14) into (8) yields

$$\frac{\partial}{\partial t}\int_{P_T}^{P_S} (K + c_pT + Lq)\ dp/g + \int_{P_T}^{P_S} \nabla \cdot (K + c_pT + Lq + gz)\vec{V}\ dp/g \qquad (15)$$

$$= SW_A + LW_S - LW_T + SH + LH$$

which is the atmospheric energy balance equation. The first term on the right hand side is the time tendency of energy stored in the atmosphere, and the second term is the flux divergence of energy.

Appendix II

Model Physics

A. Cloud parameterization

Large scale cloudiness occurs in the GLA GCM when the relative humidity at a gridpoint exceeds 100%. The sub-grid scale moist convection parameterization is based on the scheme developed for the UCLA 3-level model (Arakawa, 1972). Convection occurs when a layer is buoyant with respect to a higher layer, determined by the dry and moist static stabilities of successive layers. Cumulus clouds form where the air rises moist adiabatically. Convective clouds are termed penetrative when the lowest six layers (layers 4-9 where 9 is the lowest layer) participate in the vertical mixing. Low level convection involves layers 7 and 8 and middle level convection layers 5 and 6. Upon formation, clouds are assumed to fill the entire grid volume.

B. Radiation

The amount of shortwave radiation absorbed by the model atmosphere depends on the zenith angle of the sun, albedo of the earth's surface, humidity, and the amount and type of clouds. The concentrations of the absorbing gasses CO_2, O_2 and O_3 are prescribed by season and latitude while the distribution of water vapor is updated every time step. The optical properties of liquid water in clouds, i.e. the optical depth and albedo are prescribed, as liquid water is not a predicted model variable. The absorption of solar

radiation includes the parameterized effects of multiple scattering. These parameterizations are described by Lacis and Hansen (1974) for H_2O, Ramanathan and Cess (1974) for CO_2 and by Strobel (1978) for O_2 and O_3.

The flux of longwave radiation in the atmosphere is calculated using the Wu-Kaplan scheme (Wu, 1980) in the troposphere and the scheme developed by Apruzese et al. (1982) in the stratosphere (from 120 mb to 10 mb). The two schemes interface at 120 mb where they are joined by interpolation. The Wu-Kaplan scheme includes the effects of water vapor, CO_2, and O_3. Detailed calculations approximating the radiative transfer equations are carried out for water vapor while laboratory measurements are used to prescribe the transmission functions of CO_2 and O_3. Clouds and the ground are assumed to be blackbodies which act as vertical boundaries in the flux calculations. In the stratosphere, the absorption and emission of radiation due to CO_2 and O_3 are treated by a two-stream approximation, with the effects of water vapor assumed negligible. To increase accuracy, the number of layers is doubled and two additional layers are included between 1 and 10 mb.

The model-computed net radiation at the surface depends on the absorption of shortwave and the flux of longwave radiation. There are two formulations for the shortwave radiation, one for the wavelengths where absorption due to water is significant, and the other for the remaining wavelengths. The longwave flux is given by σT^4 where σ is the Stefan-Boltzmann constant.

C. Surface sensible and latent heat flux

The surface sensible and latent heat fluxes are computed using the following bulk aerodynamic formulae (Sud and Abeles, 1981)

$$SH = -\rho \, Dr \, c_p \, (T_{SSL} - T_S)$$

$$LH = -\rho \, Dr \, \beta \, L \, (q_{SSL} - q_S)$$

where T_{SSL} is the temperature at the top of the surface sublayer, located between 10 and 50 m above the surface. ρ is the air density in the SSL, and Dr is an air/surface interaction coefficient which depends on the surface winds, surface drag and convective instability. In the latent heat formulation, β is the soil evapotranspiration coefficient (equal to 1 over the ocean), q_{SSL} the specific humidity at the top of the surface sublayer and q_S the saturation specific humidity at the surface.

Appendix III

The Atmospheric Energy Budget in Sigma Coordinates

In sigma coordinates, the flux form of the kinetic energy equation is given by

$$\frac{\partial}{\partial t}(K\,P_S/g) + \nabla\cdot(K\vec{V}\,P_S/g) + \frac{\partial}{\partial\sigma}(K\dot{\sigma}\,P_S/g) + \vec{V}\cdot(\nabla gz + RT\,\frac{\nabla P_S}{P_S})\,\frac{P_S}{g} = \vec{V}\cdot\vec{F}\,P_S/g \tag{1}$$

and the equation sensible heat by

$$\frac{\partial}{\partial t}(c_pT\,P_S/g) + \nabla\cdot(c_pT + gz)\vec{V}\,\frac{P_S}{g} + \frac{\partial}{\partial\sigma}(P_S\,gz\dot{\sigma} + gz\sigma\frac{\partial P_S}{\partial t})\,\frac{P_S}{g} - \vec{V}\cdot(\nabla gz + RT\,\frac{\nabla P_S}{P_S})\,\frac{P_S}{g} = S \tag{2}$$

where R is the gas constant for air, $\dot{\sigma}=P/Ps$ and $\sigma=d\sigma/dt$. Combining (1) and (2) and integrating over the depth of the atmosphere yields

$$\frac{\partial}{\partial t}\int_0^1 (K + c_pT + gz_s)\,\frac{P_S}{g}\,d\sigma + \int_0^1 \nabla\cdot(K + c_pT + gz)\vec{V}\,\frac{P_S}{g}\,d\sigma = Q_{RAD} + Q_{SEN} + Q_{DIS} \tag{3}$$

where z_s is the height of the surface above sea level. The latent heat equation for an atmospheric column can be expressed as

$$\frac{\partial}{\partial t}\int_0^1 Lq\,P_S/g\,d\sigma + \int_0^1 \nabla\cdot Lq\vec{V}\,P_S/g\,d\sigma = Q_{LAT} \tag{4}$$

Summing equations (3) and (4) and using the expressions for diabatic heating developed in Appendix I gives

$$\frac{\partial}{\partial t}\int_0^1 (K + c_p T + Lq + gz_s)\,\frac{P_S}{g}\,d\sigma + \int_0^1 \nabla\cdot(K + c_p T + gz + Lq)\vec{V}\,\frac{P_S}{g}\,d\sigma = Q_{DIS} + Q_{RAD} + Q_{SEN} + Q_{LAT} \tag{5}$$

which is the energy balance equation in sigma coordinates.

In order to compare the results of the energy budget equations in pressure and sigma coordinates, the model diagnostics used in these computations are integrated over the same vertical domain. However, the model diagnostics in pressure coordinates are given between the 1000 mb and 50 mb levels, while in sigma coordinates the upper and lower diagnostic levels are σ=1/18 (~65 mb) and the surface (σ=1). To align the lower boundaries of both coordinate systems, the diagnostics generated at 1000 mb are assumed to be surface values. The upper boundaries are matched by linearly extrapolating the values at the upper most sigma levels to the sigma level corresponding to 50 mb. Vertical integrations can then be performed between the surface and 50 mb in both coordinate systems.

Acknowledgments

I wish to express my sincere gratitude to Professor Gerald Herman for his support and guidance throughout this study. I would like to thank Professors Stefan Hastenrath and John Kutzbach for their helpful comments. Drs. William Raymond and Kenneth Potter are thanked for their advice on error analysis.

I am indebted to the staff of the Modeling and Simulation Facility of the Goddard Laboratory for the Atmosphere, including Dr. Eugenia Kalnay, Mr. L. Tackas, Mr. J. Pfaendtner and Miss. M. Almeida. Special thanks go to Dr. Siegfried Schubert for providing excellent advice and assistance in developing the energy budget equations and code.

The calculations in this study were performed on the Amdahl-V6 computer at the Goddard Laboratory for the Atmospheres which is sponsored by the National Aeronautics and Space Administration. This research was supported by NASA grant NSG-5223.